

**A Proposal for a Three Detector
Short-Baseline Neutrino Oscillation Program
in the Fermilab Booster Neutrino Beam**

Part III: T600 Design and Refurbishing

January 8, 2015

CONTENTS

I. Introduction	1
II. Physics of Far Detector	3
A. The SBN experimental program	3
B. T600 Physics with the NuMI beam	3
III. Requirements for Detector Performance	4
IV. The T600 Detector: present configuration	5
A. TPC design	6
B. Light Collection system	15
C. Electronics, DAQ and Trigger	17
D. Cryogenics and Purification systems	19
V. Overhauling of the T600 Detector: WA104	24
A. TPC modifications	25
B. New Light Collection System Layout and Implementation	27
C. New Electronics, DAQ and Trigger	32
D. New Cryogenic and Purification systems	37
VI. Cosmic Ray Tagging System	42
A. CRTS efficiency	43
B. CRTS layout	44
References	45

I. INTRODUCTION

Imaging detectors have always played a crucial role in particle physics. In the past century successive generations of detectors realized new ways to visualize particle interactions, driving the advance of physical knowledge and the discovery of unpredicted phenomena, even on the basis of single fully reconstructed events. In particular, bubble chamber detectors were an incredibly fruitful tool, permitting to visualize and study particle interactions, providing fundamental contributions to particle physics discoveries. Gigantic bubble chambers, like Gargamelle [1, 2] (3 tons of mass), were extraordinary achievements, successfully employed in particular in neutrino physics. Two major limitations of bubble chambers in the search for rare phenomena are the impossibility to scale their size towards much larger masses, and their duty cycle which is intrinsically limited by the mechanics of the expansion system.

In 1977 C. Rubbia [3] conceived the idea of a Liquid argon Time Projection Chamber (LAr-TPC), i.e. the calorimetric measurement of particle energy together with three-dimensional track reconstruction from the electrons drifting in an electric field in sufficiently pure liquid argon. The LAr-TPC successfully reproduces the extraordinary imaging features of the bubble chamber, its medium and its spatial resolution being similar to those of heavy liquid bubble chambers, with the further feature of being a fully electronic detector, potentially scalable to huge masses (several kton). In addition the LAr-TPC provides excellent calorimetric measurements and has the big advantage of being continuously sensitive and self-triggering.

The ICARUS-T600 cryogenic detector is the biggest LAr-TPC ever realized, with the cryostat containing 760 tons of LAr (476 tons active mass). Its construction finalized many years of R&D studies by the ICARUS Collaboration [4–8], with prototypes of growing mass developed both in laboratory and with industry involvement. Nowadays, it represents the state of the art of this technique and it marks a major milestone in the practical realization of large-scale LAr detectors.

The pre-assembly of the ICARUS T600 detector began in 1999 in Pavia (Italy); one of its two 300-tons modules was brought into operation in 2001. A test run lasting three months was carried out with exposure to cosmic rays on the surface, allowing for the first time an extensive study of the main detector features [9]. After the test, the detector was de-commissioned and, in 2004, the two cryostats housing the internal detectors were transported to their final site, in the Hall B of the underground Gran Sasso National Laboratories (LNGS). A number of activities on the ICARUS-T600 plant were then necessary for the completion of the detector assembly in its underground site. In the first months of 2010 the T600, see Fig. 1, was finally brought into operation [10] taking data with the CERN to Gran Sasso (CNGS) neutrino beam and with cosmic rays. The ICARUS experiment has operated with a remarkable detection efficiency and it has successfully completed a three years physics program being exposed to the CNGS beam from October 2010 to December 2012. Neutrino events have been collected, corresponding to 8.6×10^{19} protons on target with an efficiency exceeding 93%. Additional data were also collected with cosmic rays, to study atmospheric neutrinos and proton decay. From the technological point of view, the T600 run was a complete success, featuring a smooth operation, high live time, and high reliability. A total of about 3,000 CNGS neutrino events has been collected and is being actively analyzed.

The successful operation of the ICARUS-T600 LAr-TPC proves the enormous potential of this detection technique, addressing a wide physics program with the simultaneous exposure to the CNGS neutrino beam and cosmic-rays [11–14]. Moreover, the solutions adopted for the argon recirculation and purification systems permitted to reach an impressive result in terms of argon purity, which is one of the key issues for the superb detector performance. A

corresponding free electron lifetime exceeding 15 ns has been obtained, a milestone for any future project involving LAr-TPCs. This result [15] demonstrates the effectiveness of the single phase LAr-TPC detectors [16, 17], paving the way to the construction of huge detectors with longer drift distances: for example, with the achieved purity level, at 5 m from the wire planes the maximum signal attenuation is only 23%.

The T600 decommissioning process started in June 2013, with the cryostat emptying phase lasting less than one month in a safe and smooth way. A warming-up phase followed, that brought the cryostats to room temperature in about one month. The T600 dismantling started in September 2013 and globally lasted about 10 months. After it was concluded, the cryostats were opened, to recover the internal TPC detectors and the cryogenic plant and electronics to be re-used in future projects.

The movement of the two T600 modules to CERN has been already completed. The ICARUS-T600 TPCs are ready for their complete overhauling (CERN WA104 project), preserving most of the existing operational equipment, while upgrading some components with up-to-date technology in view of the T600 future non-underground operation at FNAL.

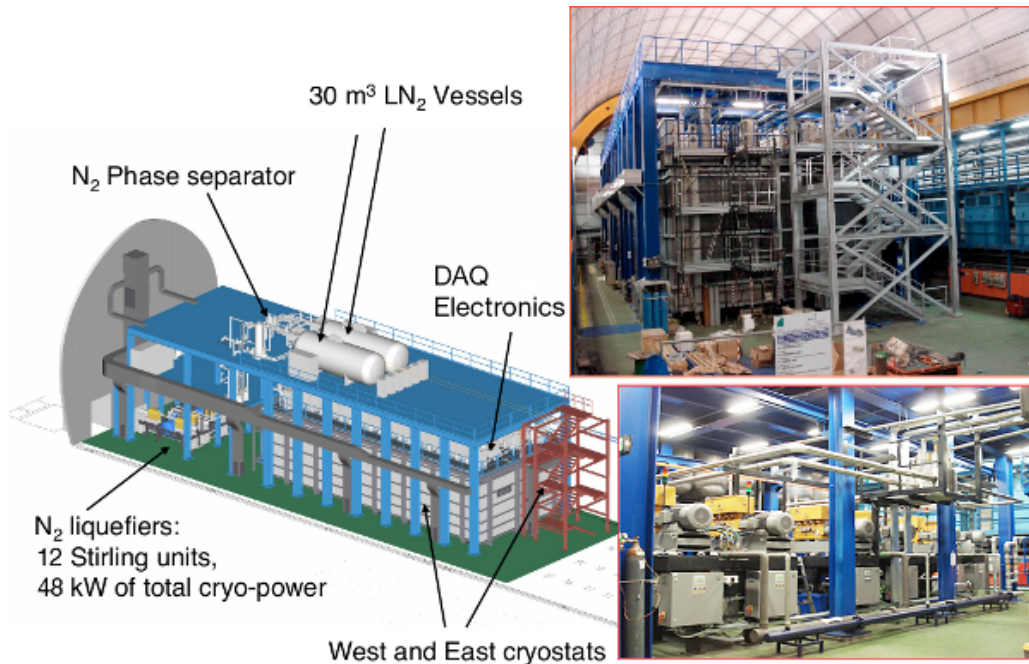


FIG. 1: Left: schematic view of the whole ICARUS-T600 plant in Hall B at LNGS. Right-top: photo of the detector installation. Right-bottom: details of the cryo-cooler plant.

This Design Report is organized as follows. Sec. II, after recalling the SBN experimental program, briefly reviews the potential of the ICARUS-T600 standalone physics program with the NuMI beam. Requirements for the detector to operate at shallow depths are resumed in Sec. III. The present ICARUS-T600 detector configuration is described in Sec. IV, while the T600 overhauling activities foreseen at CERN as WA104 program are shown in Sec. V, with particular emphasis on the new Light Collection System, the new Electronics and the new Cryogenic and Purification systems. The possibility to complement the detector with an external cosmic ray tagging system is discussed in Sec. VI.

II. PHYSICS OF FAR DETECTOR

A. The SBN experimental program

In recent years, several experimental “anomalies” have been reported which, if confirmed, could be hinting at the presence of additional “sterile” neutrino states with larger mass-squared differences participating in the mixing [18–24]. An important contribution to the sterile neutrino search has been already given by the ICARUS Collaboration with the T600 detector running in the underground INFN-LNGS Laboratory and exposed to the CNGS neutrino beam [10–12].

As already described in details in the Part I of this Proposal, the future short-baseline experimental configuration is proposed to include three LAr-TPC detectors located on-axis along the Booster Neutrino Beam (BNB). The Near Detector (LAr1-ND) will be located in a new building directly downstream of the existing SciBooNE enclosure, 110 m from the BNB target. The MicroBooNE detector, which is currently in the final stages of installation, is located in the Liquid argon Test Facility (LArTF) at 470 m. The Far Detector (the existing ICARUS-T600) will be located in a new building, 600 m from the target, between MiniBooNE and the NO ν A Near Detector surface building. The challenge of predicting absolute neutrino fluxes in accelerator beam experiments, and the large uncertainties associated with neutrino-nucleus interactions, strongly motivate the use of multiple detectors at different baselines, to reduce systematic uncertainties in the search for oscillations.

The observed set of anomalous results in neutrino physics calls for a conclusive new experiment capable of exploring the parameter space in a definitive way and to clarify the possible existence of eV-scale sterile neutrinos.

B. T600 Physics with the NuMI beam

The physics outreach of the T600 detector as a stand alone detector can be enhanced with the study of neutrino cross-sections and interaction topologies at energies relevant to the Long Baseline Neutrino Facility (LBNF) program, exploiting the off-axis neutrinos from the NuMI beam.

The NuMI beam-line is fed by 120 GeV protons with 4×10^{13} protons per pulse. The secondary beam includes a double-horn focusing system which allows for different variable energy configurations producing a neutrino beam directed, towards the far MINOS detector, with a slope of ~ 50 mrad.

Given the NuMI repetition rate (0.53 Hz) and its spill duration (8.6 μ s), one trigger every 12 s is expected in the T600, mainly due to cosmic rays occurring in the coincidence gate. About 1 neutrino event from the NuMI beam every 150 s is also foreseen.

The T600 will collect a large neutrino event statistics in the 0–3 GeV energy range with an enriched component of electron neutrinos (several %) from the dominant three body decay of secondary K . A careful and detailed analysis of these events will be highly beneficial for the future LBNF LAr program, allowing to study very precisely detection efficiencies and kinematical cuts in all neutrino channels and event topologies.

A FLUKA-based Monte Carlo simulation [25–27] of the NuMI beam line has been set up according to the available technical drawings [28] for the low energy beam configuration. The obtained neutrino fluxes have been compared with those published by the MINOS collaboration at the MINOS near detector position. Even if not all the geometry details were available and/or included in the simulation, our results agree with the MINOS ones within 20%, indicating that

reliable prediction of neutrino rates at off-axis positions is possible.

Muon neutrino event rates are comparable with the ones from the Booster beam, while the electron neutrino component is enhanced in the off-axis beam.

This amount of data would allow a detailed evaluation of detection efficiency and background reduction at the energy of the second oscillation maximum in the LBNF expected signal.

III. REQUIREMENTS FOR DETECTOR PERFORMANCE

The ICARUS-T600 detector in the present configuration is already well suited for sterile neutrino searches at FNAL. Nonetheless, it was designed for the low background, deep underground conditions of LNGS laboratory, where the single prompt trigger has always ensured the unique timing connection to the main image of the event. However, the situation will be substantially different for a detector of this magnitude if placed at shallow depths (a few meters deep), since several additional and uncorrelated triggers (due to cosmic rays) will be generally occurring continuously and at different times during the ~ 1 ms duration of the T600 readout window [29]. This represents a new problem since, to reconstruct the true position of the track, it is necessary to precisely associate the different timings of each element of the image to their own specific delay with respect to the trigger. The specific investigation of the oscillation anomalies at shallow depths is based on the search of a signal with the presence of a neutrino-induced, single ionizing electron (or positron). High energy cosmic muons creating secondary showers may also produce single ionizing background electrons or positrons with similar energies. At the neutrino energies of the FNAL Booster Beam, the intrinsic ν_e CC contamination occurs at the very low rate of ~ 500 ν_e CC/y, while a possible LSND-like oscillation signal will produce a few hundred ν_e CC/y (e.g. ~ 170 ev/y for $\Delta m^2 = 0.43$ eV², $\sin^2 2\theta = 0.013$). On the other hand, as already described in details in Part I of this Proposal, the cosmic ray background is very prolific of events: in a pit covered by 3 m of concrete, cosmic muon rates in coincidence with the beam trigger window of 1.6 μ s, will produce the huge rate of 0.83×10^6 cosmic per year (c/y). Moreover, during the 1 ms long duration of each readout window, ~ 11 cosmic ray tracks are expected over the full T600, in agreement with the ICARUS measurements at surface carried out in 2001 test run [9]. It is concluded that in its original configuration the ICARUS LAr-TPC detector cannot perform a practical search for LSND-like anomalies at shallow depths, since the cosmic trigger events are too much frequent. As already pointed out in Part I, depending on the background type, several reduction strategies can be applied. In addition to offline analysis techniques for background reduction, mostly based on electron/photon discrimination through dE/dx evaluation, the T600 detector will require the implementation of the following three features:

- the realization of a new light collection system, to allow a more precise event timing and localization;
- the exploitation of the BNB bunched beam structure, lasting 1.15 ns (FWHM ~ 2.7 ns) every 19 ns, to reject cosmic events out of bunch as proposed in a SBN note [30];
- the realization of a cosmic ray tagging system, external to the LAr fiducial volume, to automatically identify entering charged tracks with position and timing information: this would greatly facilitate the reconstruction and identification of muon tracks. It has to be reminded that crossing muons can be identified by the 3D reconstruction software, however the 3D reconstruction itself needs the information on the track absolute time t_0 .

IV. THE T600 DETECTOR: PRESENT CONFIGURATION

The ICARUS-T600 detector consists of a large cryostat split into two identical, adjacent modules, with internal dimensions $3.6 \times 3.9 \times 19.6 \text{ m}^3$ each, filled with about 760 tons of ultra-pure LAr. The modules will be referred in the text as *West module* (the oldest one) and *East module* (the newest one), with respect to CNGS beam coming from the North. A uniform electric field ($E_{drift} = 500 \text{ V/cm}$) is applied to the LAr bulk: each module houses two TPCs separated by a common cathode.

Charged particles, generated for example by a neutrino interaction in LAr, produce ionization along their path. Thanks to the low transverse diffusion of charge in LAr, the images of the tracks (produced by ionization electron clouds) are preserved and, drifting along the electric field lines, are projected onto the anode, as illustrated in Fig. 2. The TPC anode is made of three parallel planes of wires, 3 mm apart, facing the 1.5 m drift path. Globally, 53,248 wires with length up to 9 m are installed in the detector. By appropriate voltage biasing, the ionization charge induces signals in non-destructive way on the first two planes (Induction-1 and Induction-2), then it is finally collected by the last one (Collection plane).

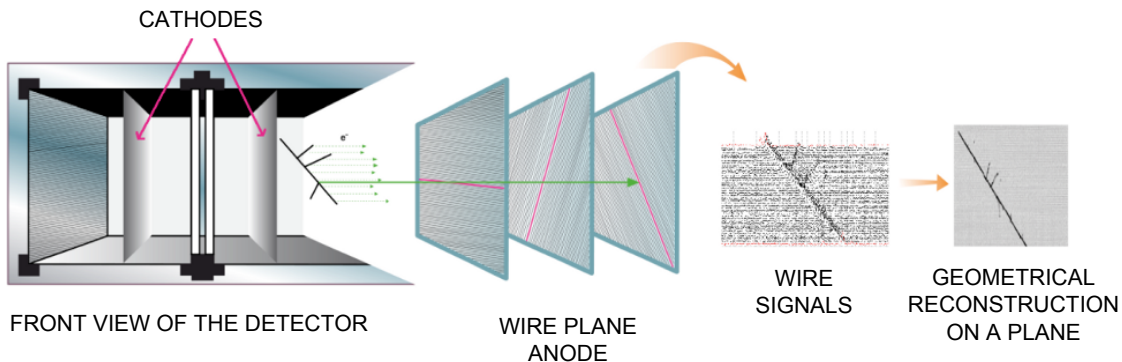


FIG. 2: Illustration of the ICARUS-T600 working principle: a charged particle ionization path in LAr and its geometrical reconstruction.

Wires are oriented on each plane at a different angle (0° , $+60^\circ$, -60°) with respect to the horizontal direction. Therefore, combining the wire/drift coordinates on each plane at a given drift time, a three-dimensional reconstruction of the ionizing event can be obtained. A remarkable resolution of about 1 mm^3 is uniformly achieved over the whole detector active volume (340 m^3 corresponding to 476 t).

The measurement of the absolute time of the ionizing event, combined with the electron drift velocity information ($v_{drift} \sim 1.6 \text{ mm}/\mu\text{s}$ at $E_{drift} = 500 \text{ V/cm}$), provides the absolute position of the track along the drift coordinate. The determination of the absolute time of the ionizing event is accomplished by the prompt detection of the scintillation light produced in LAr by charged particles. To this purpose, arrays of cryogenic Photo Multiplier Tubes (PMTs), coated with wavelength shifter to allow the detection of Vacuum Ultra-Violet (VUV) scintillation light ($\lambda = 128 \text{ nm}$), are installed behind the wire planes.

The electronics was designed to allow continuous read-out, digitization and independent waveform recording of signals from each wire of the TPC. The read-out chain is organized on a 32-channel modularity. A Decoupling Board receives the signals from the chamber and passes them on to an Analogue Board via decoupling capacitors; it also provides wire biasing voltage and the distribution of the test signals. Digitization is performed by 10-bit fast ADCs, which

continuously read data and store them in circular buffers. Stored data are read out by the DAQ when a trigger occurs. The trigger relies on the detection of scintillation light by the PMTs, in coincidence with the CERN-SPS proton extraction time for the CNGS beam.

This Section is organized as follows: Par. IV A describes in details the main component of the ICARUS-T600 internal detectors: the mechanical structure, the wire planes, the cabling and the High Voltage system. Par. IV B shows the present layout of the Light Collection System, while the Electronics and DAQ in the LNGS configuration are described in Par. IV C. Finally, Cryogenics and Purification systems are presented in Par. IV D.

A. TPC design

1. TPC mechanical structure

Each one of the two LAr cryostats hosts a mechanical structure that sustains the different internal detector subsystems and the control instrumentation, namely: (1) the TPC wire planes and the relative HV electrode system (cathode and field-shaping electrodes), (2) the PMT system for the scintillation light detection and (3) sensors and probes of the slow control system. Once the cryostat is filled, the structure is totally immersed in LAr.

All materials of the mechanical structure were chosen and treated to guarantee high LAr purity and minimal radioactive contamination: the main components (beams and pillars) have been built with AISI 304L stainless steel; other parts (supports, spacers, etc.) are made of PEEK™. The stainless steel structure has dimensions of 19.6 m in length, 3.6 m in width and 3.9 m in height, for a total weight of ~ 20 tons, see Fig. 3 and 4.

To cope with the different thermal shrinking between aluminum and stainless steel, the stainless steel structure leans on the cryostat aluminum floor by means of 10 adjustable feet positioned on corresponding reinforced pads, and rigidly linked to it only in two pads at half-module length. In this way, the structure is practically independent from deformations of the cryostat induced by cooling and by the different operating conditions (vacuum and overpressure). Moreover, the sustaining structure is self-supporting and is rigid enough to allow for transportation.

Rocking frames to hold the TPC wires are positioned on the vertical long sides of the mechanical structure. The latter was dimensioned in such a way to sustain the total mechanical tension of the wires applied to the two wire frames, whose design is based on the concept of the variable geometry design (weight bridge). This is based on movable and spring loaded frames, to set the proper tension of the wires after installation, see Fig. 5 and Fig. 6. This system allows for a precise detector geometry and planarity, compensating for any possible over-stress during the cool-down and LAr filling phases, and counteracting the flexibility of the structure.

2. TPC wire planes

The anode of each TPC consists of a system of three parallel wire planes (of 17.95×3.16 m² surface), 3 mm apart from each other, for a total of 13312 wires/chamber, see Fig. 7; a total of 53,248 wires is mounted on the whole T600 detector (four chambers). Wires are made of AISI 304V stainless steel with a wire diameter of 150 μ m; wire length ranges from 9.42 m to 0.49 m depending on the position of the wire in the plane itself. Thirteen windings (slipknots) around two gold-plated stainless steel ferrules at both ends of each wire are realized, in a "guitar chord"

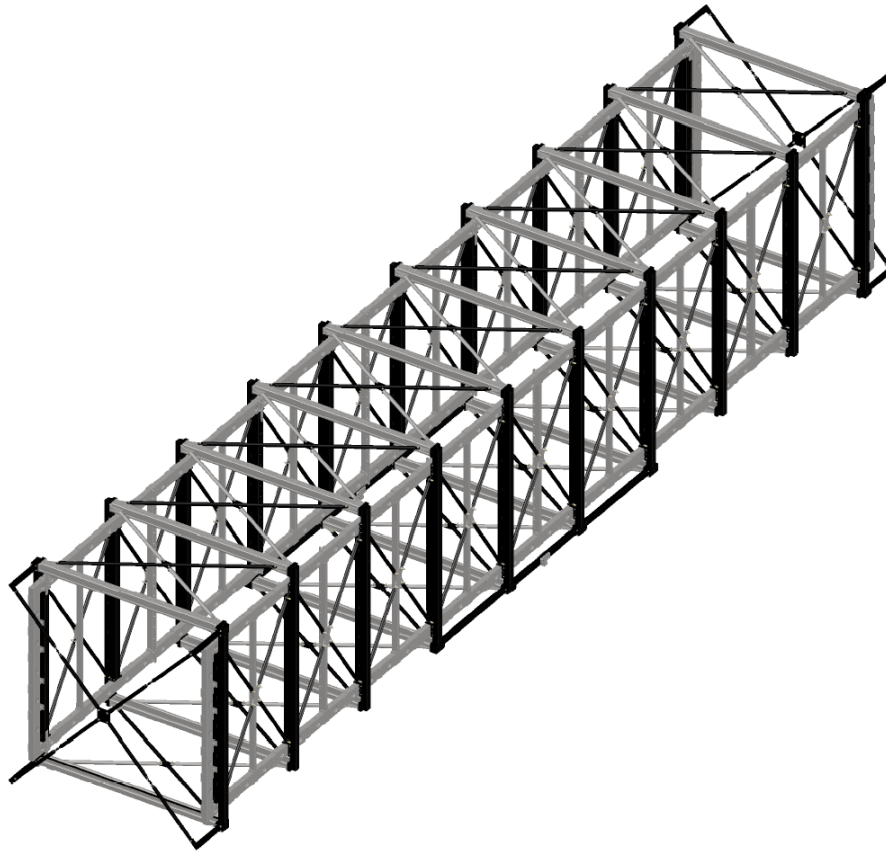


FIG. 3: Drawing of the bare inner mechanical structure of one T600 module, working as a support for all the internal detector subsystems.

configuration, see Fig. 8. In this way a very safe holding is guaranteed by the wire friction itself. From the mechanical point of view, wires are strung with a nominal tension of 12 N (5 N for the longest wires), which is high enough to limit sagittas (due to gravity and to electrostatic forces) to values negligible with respect to the distance between the wires. The wire elongation is still well below the elastic limit (39 N nominal value).

The variable geometry design demonstrated its reliability since none of the wire broke and no damages at the wire chamber structure occurred: in the 2001 Pavia test run; during the transport of the two modules from Pavia to LNGS; during all the installation movements on site; during the commissioning, run and de-commissioning at LNGS. The wires are stretched in the elastic frame sustained by the mechanical structure, as described above. Two coplanar, adjacent sets of horizontal wires (1056 units), 9.42 m long, form the Induction-1 plane, stretched between the vertical beams of the wire frame and a central fixed beam. For both the Induction-2 and Collection planes (wires inclined at $\pm 60^\circ$) the standard length of the wires stretched between the upper and lower beams of the frame is 3.77 m (4640 wires per plane), whereas wires of decreasing length (960 wires per plane) are used in the triangular-shaped portions, between one vertical and one horizontal beam, at the corners of the planes (Fig. 6). The single wire capacitance in the various planes has been calculated to be 20 pF/m for the first (Induction-1) and third (Collection) plane, and 21 pF/m for the intermediate (Induction-2) plane.

The wires are anchored by special holders onto the wire frame in groups of 32 units (the *wire modules*). Each holder is formed either by one or two (according to the different cases)



FIG. 4: *The internal sustaining structure of a T600 module.*



FIG. 5: *Detail of the wire tensioning mechanics: a 2 m long portion of the wire frame equipped with three tensioning springs.*

PEEK™ combs contained in stainless steel supports which also embed one or two printed circuit boards. The wire ferrules, held by the PEEK™ shell at both ends of the wire module, are hung on the comb pins. The printed circuit board establishes the electric connection between the 32 pins of the comb and a single connector also mounted onto the board. Fig. 9 shows the technical design of the mechanical system holding 2 wire modules for the wires at $\pm 60^\circ$.

The wire modules are individually mounted onto the beams of the elastic frame (de-tensioned position). The elastic frame is schematically subdivided into portions about 2 m long. Each

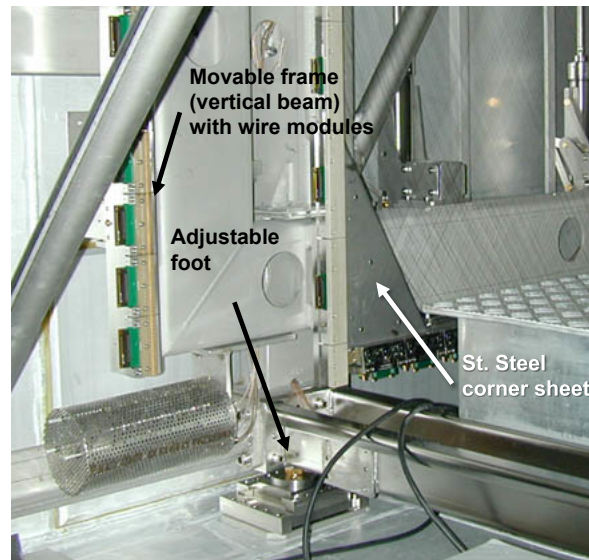


FIG. 6: Detail of the internal structure showing an adjustable foot and the wires at the corner.

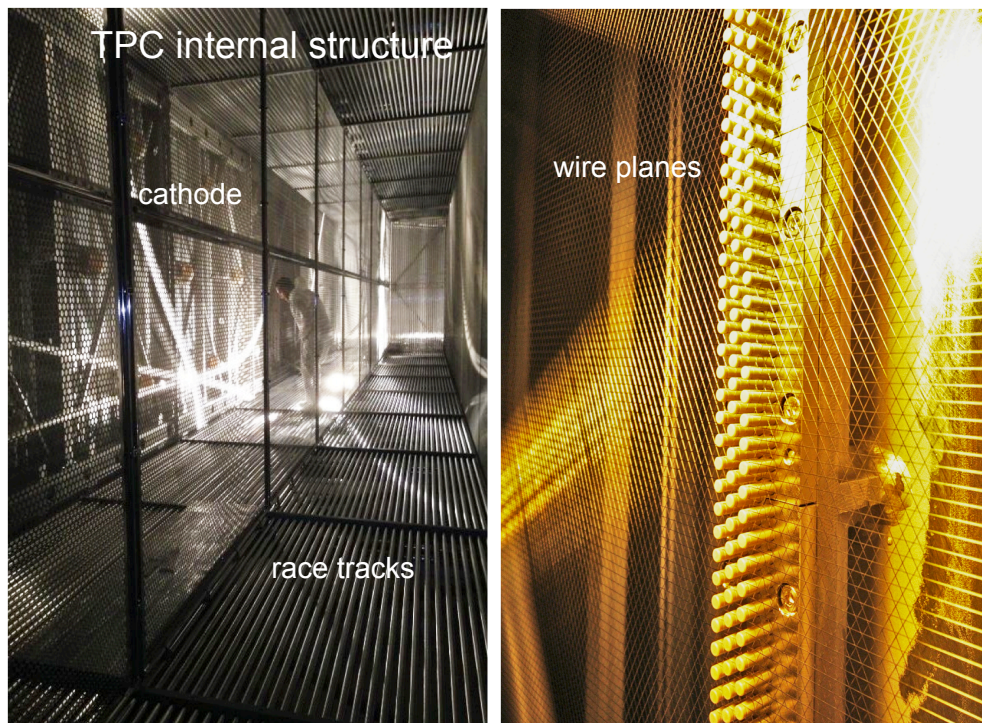


FIG. 7: Left: internal TPC structure: cathode, race tracks and wire planes are highlighted. Right: detail of the three wire plane structure.

portion comprises 18×2 combs/connectors. After the installation of the wire modules was completed, wires were tensioned by loading the springs of the movable frame, see Fig. 5.

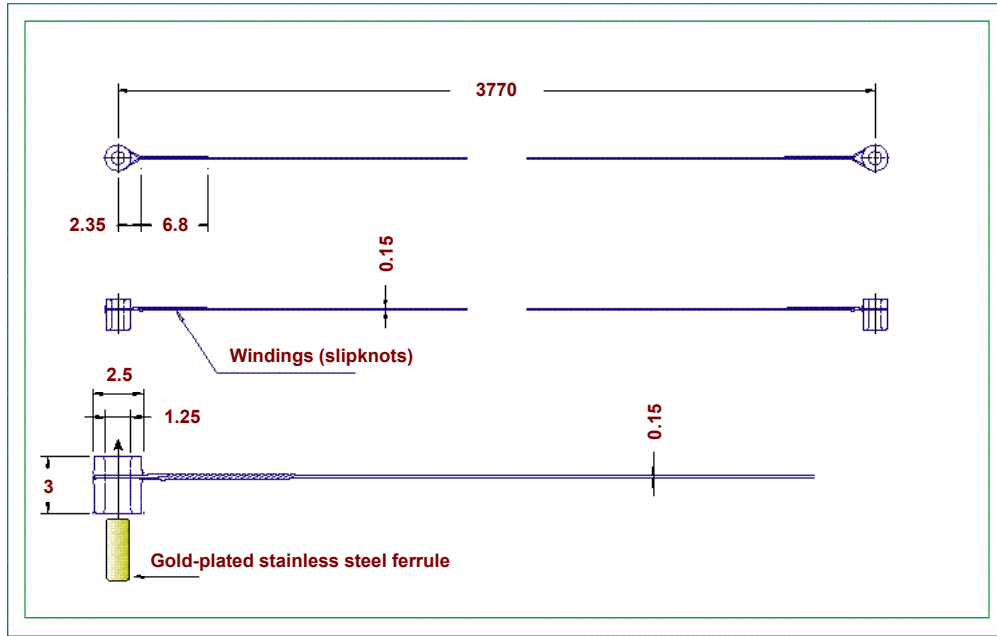


FIG. 8: Schematic of the Wire holding structure, with detail of the winding in a "guitar chord" concept.

3. Cabling

The individual wire signal transfer to the read-out electronics outside the cryostat is provided by twisted-pair flat cables (34 pairs, flexible, halogen free). Thirty-two pair lines (pairs 1÷32) of the 68 available contacts are dedicated to wire signals, one to the test-pulse signal and the last pair, referred to ground, is used as a screen between signal and calibration conductors. Inside the cryostat the flat cables, suitably terminated with male connectors at both ends, are plugged at one end to the female connectors (32-wire channels + 1 test pulse channel + 1 screen channel) mounted onto the printed boards of the wire modules. At the other end, the cables are plugged to similar connectors embedded (inner side) in specially designed vacuum tight feed-through flanges. Flanges are mounted on the top of the cryostat, at the end of the way-out chimneys. Each one of the 96 feed-through flanges installed in the T600 detector can provide signal transmission for 18 wire modules (576 wires) and for cables for test pulse calibration. The complete connection layout from wires to the read-out electronics is schematically displayed in Fig. 10. A refurbishment of the internal detector cabling is foreseen during the T600 overhauling activities at CERN, see Par. V.

4. TPC HV system

The HV system has to produce a stable and uniform field over the $1.50 \times 3.16 \times 17.95 \text{ m}^3$ entire drift volume. The system is made of several components, the most important of which are the cathodes, the field-shaping electrodes and the HV feed-throughs.

In the present configuration the cathodes are built up by an array of nine panels (Fig. 11 and Fig. 12) made of pierced stainless steel sheets. This solution implies an optical transparency between the two drift regions, which allows the detection of the scintillation light by means of

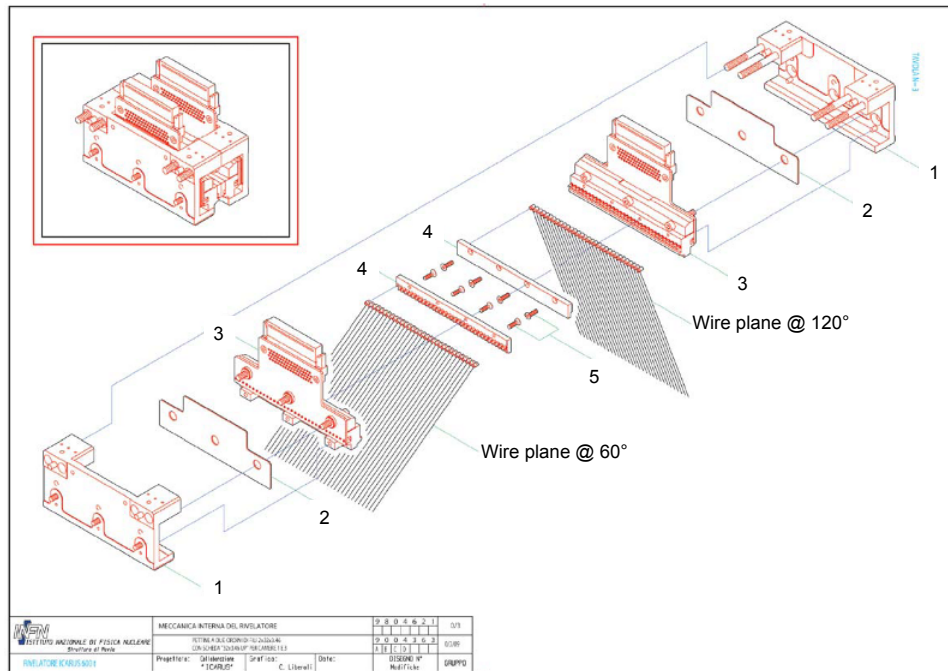


FIG. 9: Technical design of the mechanical system holding the 32-wire modules at $\pm 60^\circ$: detail of the components (from left to center and reverse): mechanical support, spacer, printed board with connector, PEEK™ shell with 32-wire ferrules, PEEK™ comb (and reverse).

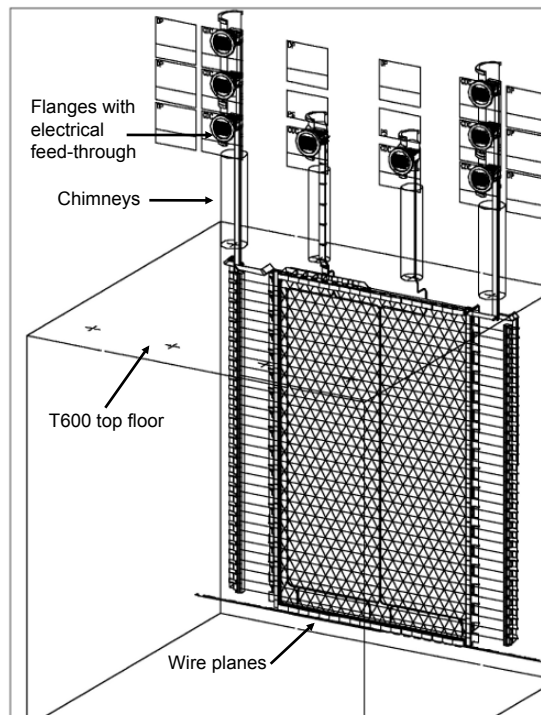


FIG. 10: Wires, cables, chimney and feed-through layout. The back side of the electronic racks (LNGS configuration) is indicated. Note that the wire chamber longitudinal dimension is not in scale, i.e. the figure includes only the non-repetitive portions of the TPC.

all PMTs positioned between the wire chambers and the cryostat walls.



FIG. 11: *Detail of one cathode panel in the LNGS run configuration.*

The electric field in each drift volume is kept uniform by means of the field-shaping electrodes (*race tracks*, see Fig. 13 and Fig. 14). These consist of 29 rectangular rings ($18.1 \times 3.2 \text{ m}^2$) for each wire chamber, made of 2 m long stainless steel tubular elements (34 mm diameter, 0.8 mm thick) connected by two welded terminals. The distance between race tracks is 49.6 mm. In the upper part, between the race tracks and the gaseous Ar (GAR) phase, a grounded metallic shielding is interposed. The race tracks are set at a potential linearly decreasing from the cathode value to the first wire plane voltage, to ensure uniform electric field and hence constant drift velocity inside the volumes. The biasing potentials of the race tracks are obtained through resistive voltage degraders. The HV degrader is based on four resistor chains, one for each drift volume, with the “hot” end connected to the cathode and the “cold” end set to ground. Resistor chains are made of 30 steps. Intermediate contacts are connected to the field-shaping electrodes. The resistance for each step is $25 \text{ M}\Omega$, obtained by connecting four $100 \text{ M}\Omega$ resistors in parallel. For a 0.5 kV/cm drift field the voltage across each resistor is 2.5 kV.

The HV generated by an external power supply is brought to the internal cathode via an hermetic feed-through. A feed-through coaxial geometry has been adopted: the design is based on an inner conductor (HV) and an outer conductor (ground) insulated by UHMW PE (ultra-high-molecular-weight polyethylene) as shown in Fig. 15. The outer conductor, made of a stainless steel tube, surrounds the insulator extending inside the cryostat up to the LAr level. By such a geometry the electric field is always confined in regions occupied by high dielectric strength media (UHMW PE and LAr). The inner conductor is made of a thin wall stainless steel tube, to minimize the heat input and to avoid the creation of argon gas bubbles around the HV lower end. A female contact, welded at the upper end for the connection to the HV cable, and a round-shaped elastic contact for the connection to the cathode, screwed at the lower end, complete the inner electrode. Special care has been taken in the assembling to ensure the complete filling with the PE dielectric of the space between the inner and the outer conductors and to guarantee leak tightness at ultra-high-vacuum level.

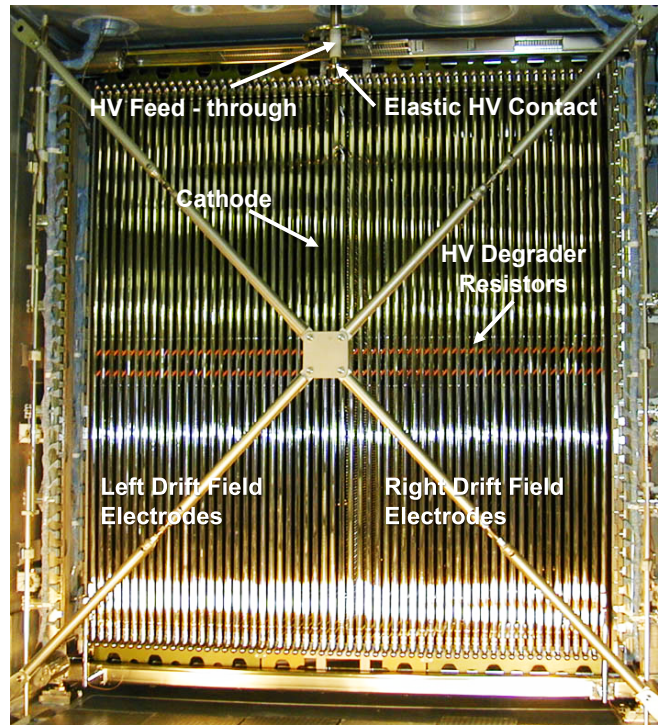


FIG. 13: The first half-module of the T600 detector before closing. Some components of the HV system are visible: feed-through, cathode, field electrodes (race tracks), voltage divider.

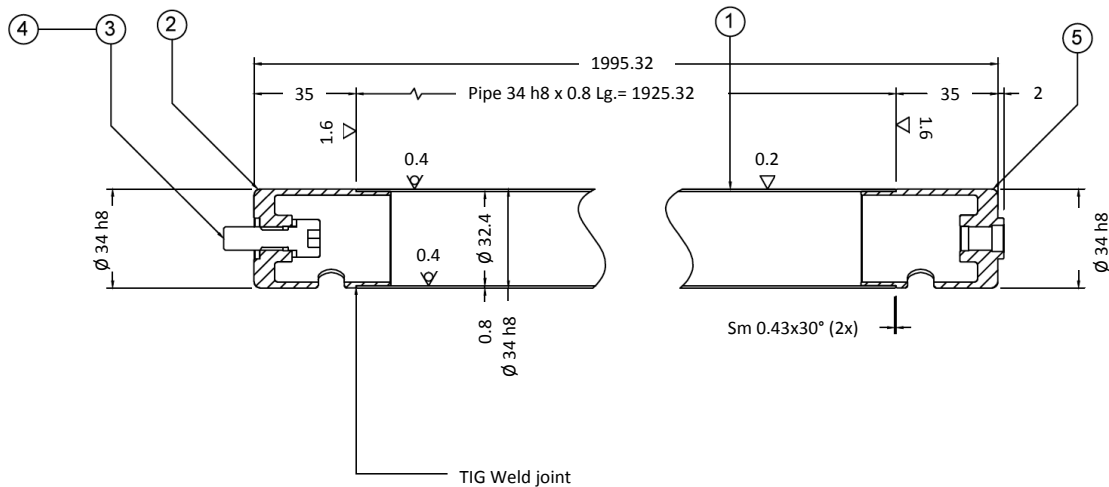


FIG. 14: Technical drawing of one race track element.

The HV system of ICARUS-T600 had no failures during the three years of run at LNGS, at the operating voltage of 76 kV. Moreover, in the last days of the LNGS run few tests were carried out with an operating voltage about twice its nominal value (150 kV, corresponding to $E_{drift} \simeq 1$ kV/cm), with no failures for five days. After this the HV system was switched off to allow the T600 decommissioning procedures to start.

The main characteristics of the present T600 TPC internal detector configuration are re-

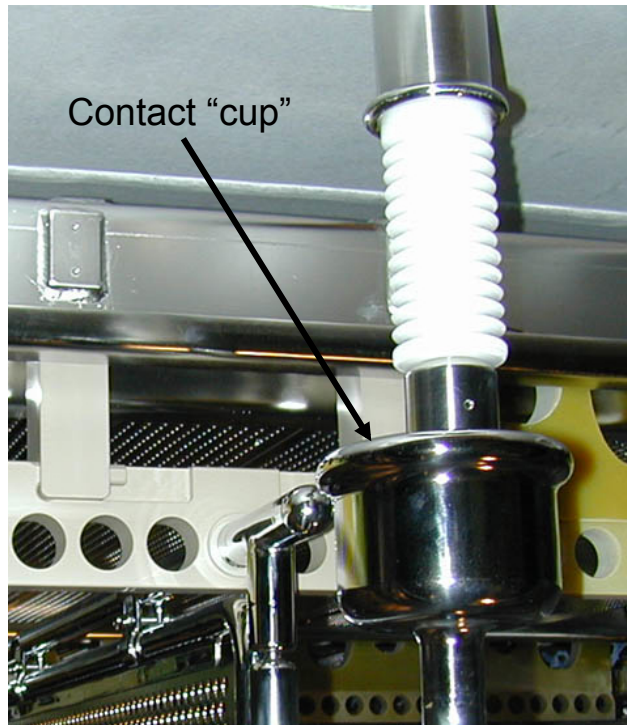


FIG. 15: Picture of the HV feed-through. The "cup" for the contact to the cathode panels is also visible.

sumed in Tab. I.

B. Light Collection system

Charged particles deposit energy in liquid argon mainly by excitation and ionization of Ar atoms, leading to scintillation light emission and free electron production, respectively. Additional scintillation light comes from the recombination of electron-ion pairs, which is inversely proportional to the strength of the electric field applied to the detector active volume. As a consequence, free-electron yield rises with the field value while photon yield decreases. In both cases saturation occurs, for minimum ionizing particles, at $E_{drift} > 10$ kV/cm. At the nominal drift field applied in ICARUS-T600, approximately the same amount of photons ($\sim 4,000$ γ /mm) and free electrons ($\sim 5,000$ ion-electron pairs per mm) are produced for minimum ionizing particles (m.i.p.) [31].

Scintillation light emission in LAr is due to the radiative decay of excited molecules (Ar_2^*) produced by ionizing particles, releasing monochromatic VUV photons ($\lambda \sim 128$ nm) in transitions from the lowest excited molecular state to the dissociative ground state. A fast ($\tau \sim 6$ ns decay time) and a slow ($\tau \sim 1.6$ μs) components are emitted; their relative intensity depends on dE/dx , ranging from 1:3 in case of minimum ionizing particles up to 3:1 in case of α -particles. This isotropic light signal propagates with negligible attenuation throughout each TPC volume. Indeed, LAr is fully transparent to its own scintillation light, with measured attenuation length in excess of several tens of meters and Rayleigh-scattering length of the order of 1 m. Because of their short wavelength the scintillation photons are absorbed by all materials inside the detector without reflection.

Number of read-out chambers (TPC) in T600	4
Number of wire planes per chamber	3
Distance between wire planes	3 mm
Wire orientation with respect to horizontal	$0^\circ, \pm 60^\circ$
Wire diameter	150 μm
Wire length	
Horizontal wires	9.42 m
Wires at $\pm 60^\circ$	3.77 m
Wires at the corners ($\pm 60^\circ$)	3.81-0.49 m
Wire pitch (normal to the wire direction)	3 mm
Wire capacitance Ind.-1, Ind.-2, Coll.	20, 21, 20 pF/m
Wire nominal tension	12 N (5 N for hor. wires)
Number of wires/wire module	32
Number of wire modules/chamber	
Horizontal wires	66
Wires at $\pm 60^\circ$	2×145
Wires at the corners $\pm 60^\circ$	2×30
Number of wires/chamber	
Horizontal	2112
At $\pm 60^\circ$	2×4640
At the corners ($\pm 60^\circ$)	2×960
Total	13312
Total number of wires in T600	53,248
Wire plane voltage biasing (typical)	-220 V, 0 V, +280 V
Cathode HV (nominal)	75 kV
Cathode to Collection plane distance	1.50 m
Sensitive volume/chamber	85 m ³
Length	17.95 m
Width	1.50 m
Height	3.16 m
Maximum drift length in LAr	1482 mm
Maximum drift time in LAr (at nominal field)	950 μs

TABLE I: *Main characteristics of the ICARUS-T600 TPCs.*

The design of the T600 detector PMT system, in the LNGS configuration, resulted from dedicated R&D activities on the LAr scintillation light detection, carried on during the second half of the 90's [7]. The adopted solution is based on the large surface Photo-Multiplier 9357FLA Electron Tube, a 12-stage dynode PMT with hemispherical glass window 200 mm (8") diameter, manufactured to work at cryogenic temperatures [32]. The PMT sensitivity to VUV photons (128 nm) was achieved by coating the glass window with Tetra-Phenyl-Butadiene (TPB), which acts as fluorescent wavelength shifter from VUV wavelengths to the PMT sensitive spectrum. A TPB coating of thickness 0.2 mg/cm² on sand-blasted glass guarantees a conversion efficiency better than 90% and good adhesion after immersion in LAr, resulting in a PMT response with

4% overall quantum efficiency [33].

PMTs are located in the 30 cm space behind the wire planes of each TPC, at 5 mm distance from the Collection wires, with a dedicated sustaining structure specially designed to compensate the thermal stresses occurring during the cooling of the T600 cryostat (Fig. 16 Left). Three rows of 9 PMTs, spaced by 2 m, found place in the East module behind each wire chamber for a total amount of 27+27 photo-devices. In the West module only the two central rows were deployed; two additional PMTs were placed in the top and bottom positions in the Right chamber at the center of the longitudinal direction, for an overall amount of 20 PMTs (Fig. 16 Right). Despite the small number of PMTs deployed inside the T600 detector in the LNGS configuration, the PMT system allowed to get a 100% trigger efficiency for CNGS-induced events above 300 MeV of deposited energy, with a remarkable stability during the three years of data taking [34].

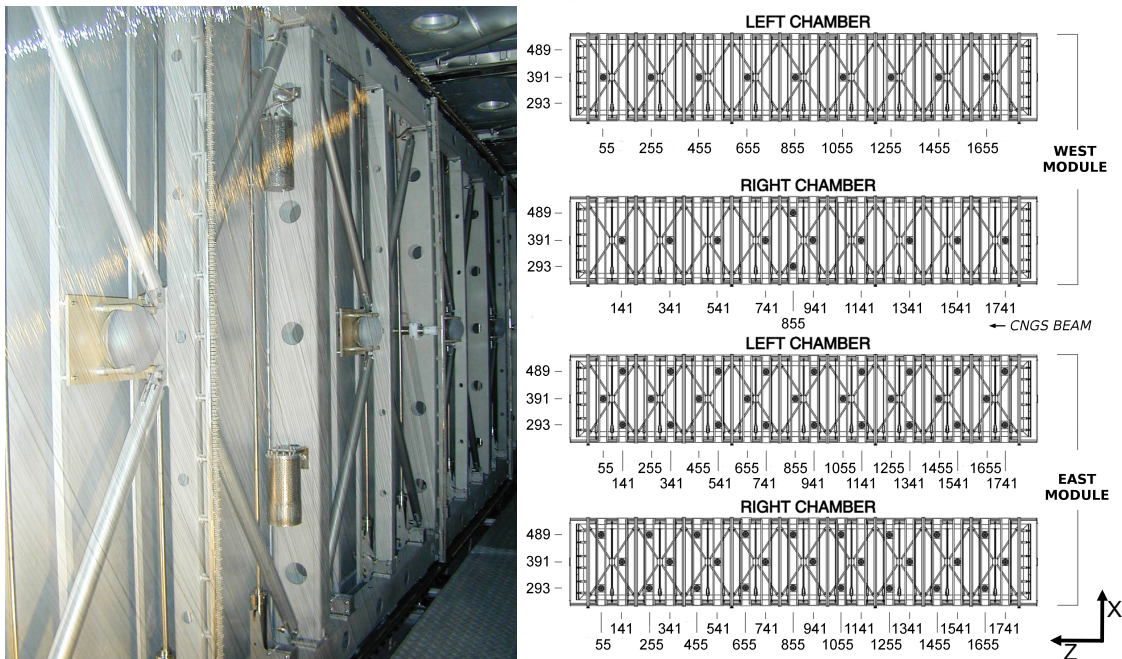


FIG. 16: *Left: internal view of one TPC, with a few PMTs clearly visible together with their sustaining structure. Right: PMTs deployment in the two ICARUS-T600 cryostats. PMT coordinates in cm are related to the reference frame used in Hall B.*

C. Electronics, DAQ and Trigger

1. Electronics and DAQ

The present T600 electronics is designed to allow continuous read-out, digitization and independent waveform recording of signals from each wire of the TPC. The read-out chain is organized on a 32-channel modularity. A Decoupling Board receives the signals from the chamber and passes them to an Analogue Board via decoupling capacitors; it also provides wire biasing voltage and the distribution of the test signals.

The Analogue Board hosts the front-end amplifiers and performs 16:1 channel multiplexing and 10-bit ADC digitization at 400 ns sampling time per channel. The overall gain is about 1,000 electrons per ADC count, setting the signal of minimum ionizing particles to 15 ADC counts, with a dynamic range of about 100 times the signal of one m.i.p. A $3 \mu\text{s}$ decay constant is used for the unipolar signals coming from the Collection and Induction-1 wires, while a $100 \mu\text{s}$ decay constant is used for the bipolar current signals (Induction-2 wires). A digital Board hosts a 10 bit waveform recorder, which continuously reads the data, stores them in multievent circular buffers, each covering a full drift distance. When a trigger signal occurs, the active buffer is frozen, following data are written to the next free buffer, and the stored data are read out by the DAQ. This configuration guarantees no dead time, until the maximum DAQ throughput (1 full-drift event per second) is reached. The average electronic noise achieved with the specially designed low noise front-end is well within expectations: 1,500 electrons r.m.s. to be compared with 15,000 free electrons produced by a minimum ionizing particle in 3 mm ($S/N \sim 10$).

2. LNGS run Trigger

Two different trigger systems based on the detection of scintillation light and ionization charge produced by charged particles in LAr have been realized for the ICARUS-T600 detector LNGS run [34]. They exploited the PMT system and the new S-Daedalus FPGA boards, spanning few orders of magnitude in event energy deposition. The main ICARUS-T600 trigger for detecting CNGS beam related events required the coincidence of the PMT *local trigger* in at least one of the four TPC chambers with a $60 \mu\text{s}$ gate opened in correspondence of the proton spill extraction delayed for the ~ 2.44 ms CNGS neutrino time-of-flight. The mentioned PMT local trigger is obtained, separately for each TPC, as the linear sum of the collected PMT signals, properly discriminated in order to account for the different number of devices deployed in the two modules.

The combined analysis of the performance of the PMT and S-Daedalus independent trigger systems demonstrated an almost full PMT trigger efficiency for CNGS neutrino events above 300 MeV energy deposition on the full T600 active volume. Efficiency remains at $\sim 98.5\%$ down to 100 MeV. The stability of the trigger system was verified within the measurement uncertainty, comparing different data sets collected during the CNGS run [34].

The T600 LNGS run Trigger Manager, built in a commercial National Instrument PXI crate, handled the different trigger sources: scintillation light collected by PMTs, timing synchronization with the CNGS extractions, charge signal collected on wires and test pulses for calibration. The system consisted of a Real Time (RT) controller (PXIe-8130) and two FPGA boards (PXI-7813R and PXI-7833). The RT controller implemented all the features that implied communication with external devices, such as the DAQ process or the CNGS Early Warning reception. Communication with the DAQ was implemented in handshake between the DAQ main process and the trigger manager. The RT controller also monitored the number of available buffers in the digital boards and prevented the generation of new triggers in case all the buffers were full. The maximum number of buffers available for full drift recording was 8. The DAQ throughput, for full drift event recording, was limited to 0.8 Hz mainly because of the adopted VME architecture. The FPGA boards implemented time critical processes, like the synchronization with the LNGS time, the opening of CNGS gate and the time stamp of each trigger. They also kept record of the trigger source and the trigger mask, monitored trigger rates from each source and controlled the overall system stability.

In the architecture of the ICARUS-T600 DAQ system adopted for data taking at LNGS [34],

all the 96 readout units work autonomously pushing their own data to 4 receiving workstations, one per TPC chamber. This segmentation and parallelization of the data stream allowed reaching a ~ 1 Hz building rate on the whole T600, safely exploiting the data link at half of the ~ 50 MB/s available bandwidth.

D. Cryogenics and Purification systems

The ICARUS-T600 cryogenic plant was mainly installed in the North end of Hall B of LNGS, i.e. behind the cryostat when entering the Hall. The final design of the system was driven by compliance to strict requirements on efficiency, safety, anti-seismic constraints and reliability for several years of operations in a confined underground location. A schematic view of the apparatus has been shown in Fig. 1 Left. The technical requirements for the plant, and its components, were developed requesting fulfillment of strict conditions in terms of mechanics, electronics, radiochemical and electronegative purity, and are summarized below:

- full cryogenic containment for safety needs;
- extremely high LAr purity: residual contamination of electronegative molecules such as water and oxygen lower than 0.1 part per billion, to allow ionization electrons to drift over several meters;
- extremely precise control of the components differential temperature during detector cool-down, in order to avoid stresses on the TPC precision mechanics. In particular the requests were of $\Delta T < 50$ K on the wire-chamber structures, $\Delta T < 120$ K on the cold vessels;
- fast cooling to liquid argon temperature, to ensure good starting purity;
- very high temperature uniformity in steady state conditions ($\Delta T < 1$ K in the main volume) to guarantee uniform electron drift velocity;
- thermal losses as low as possible, to reduce operation costs and minimize power consumption in emergency situations;
- very high stability and operation reliability to fulfill the strict underground safety requirements (this point will be re-discussed to fit the different FNAL safety standards and rules);
- full redundancy, to assure uninterrupted operation over several years.

The T600 detector is made by two adjacent aluminum LAr containers (parallelepipedal in shape), each with an inner volume of 275 m^3 . The two modules are independent from the point of view of LAr containment and purification plants, while nitrogen cooling system and thermal insulation are common to both. The main design and construction of the cryostats was carried on in collaboration with Air Liquide Italia Service (ALIS) Company [35]. The two cold vessels containing the TPCs are realized with 15 mm thick aluminum honeycomb panels, mechanically reinforced by extruded profiles. The external and internal skins work as double cryogenic containment. The external dimensions of the vessels are $4.2 \times 3.9 \times 19.9 \text{ m}^3$, i.e. the maximum size allowed for fitting the boxes into the LNGS underground laboratory. This

solution, though unconventional, was preferred mainly for its lightness and rigidity to stand stresses during the emptying phase, and the overall LAr and detector weight. A single thermal insulation vessel surrounded the two modules. The insulation was designed to behave as an additional tight container in case of cryogenic liquid spillages. Every insulation wall is composed of separated metallic boxes, with outer skin made of stainless steel. The inner and side skins are instead of Pernifer™, to avoid thermal shrinking. The boxes were filled with insulating honeycomb panels (0.4 m thick of Nomex™ or equivalent material) and super-insulation layers placed on the inner cold surface.

A thermal shield was placed between the insulation vessel and the aluminum containers, to intercept the residual heat losses through the insulation walls, thus avoiding boiling of the LAr bulk. Boiling nitrogen was circulated in the thermal shield, with a gas/liquid ratio equal to 1:5. This solution guarantees a fast cooling-down phase with thermal gradients within specification, and it forces LAr de-stratification during normal operations, thus maintaining uniform and stable temperature in the LAr bulk.

The argon and nitrogen circulation lines will be now detailed in the following, while a comprehensive view of the cryogenic system is drawn in Fig. 17.

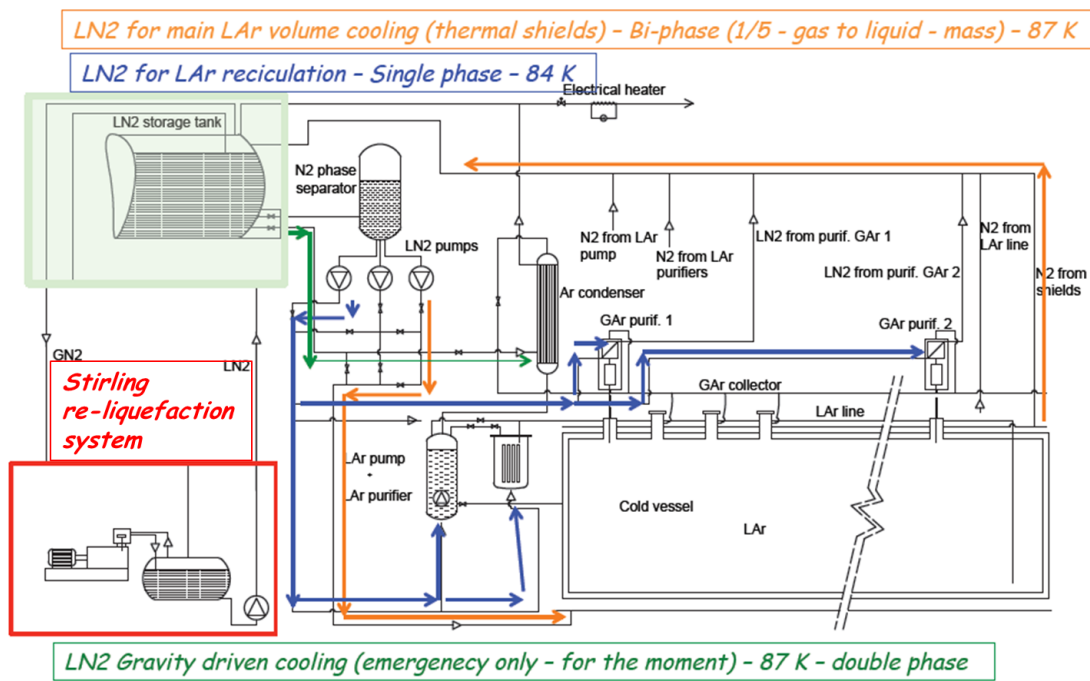


FIG. 17: Drawing of the existing plant of the ICARUS-T600 detector, containing all main elements of the system: LN₂ lines and storage tanks, GAr/LAr recirculation, Stirling re-liquefaction system. LN₂ lines are color-coded for clarity.

In order to maintain high LAr purity in the active volume, each T600 module is equipped with two GAr and one LAr recirculation units. The gas recirculation system collects argon gas coming from the chimneys hosting the read-out cables and the feed-through flanges. The gas on the T600 top is warm and dirtier than the liquid from being in contact with hygroscopic plastic cables; moreover it could be further polluted by possible small leaks due to the presence of several joints on each chimney. The collected gas is re-condensed and then made to drop into

a LN₂-cooled Oxysorb™ filter, placed after the re-condenser. Newly purified LAr is injected back into the main volume right below the liquid/gas interface. The condenser is normally fed with LN₂ at the temperature required for efficient re-condensation of the gas, by means of forced circulation.

During LNGS data taking, gas recirculation was usually kept at the maximum available rate of 25 GAr Nm³/h/unit. Gas recirculation is specially helpful during the filling phase, as it allows purification of the dirty warmer gas, while the outgassing rate decreases exponentially with temperature. On the other hand the system acts as detector pressure stabilizer during steady state operations.

Continuous liquid recirculation is used to massively purify LAr and to reach and maintain purity levels as high as possible after initial filling. It can also be exploited to rapidly restore argon purity in case of accidental pollution during operations. LAr is extracted from the main volume at about 2 m below the liquid surface on one of the 4 m long sides of the T600 modules (endcaps); it is then reinjected on the opposite side, 20 m apart, at the module floor level, through a horizontal pierced pipe that provides uniform distribution over the vessel width. Recirculation is forced by means of immersed cryogenic pumps placed inside independent dewars. Before reinjection, LAr is sent through a battery of four Oxysorb/Hydrosorb™ filter cartridges, connected in parallel. Each set of filters has a nominal O₂ absorption capacity exceeding 200 normal liters, which is enough to purify an entire module, starting from standard commercial liquid argon (O₂ concentration \sim 0.5 ppm). The maximum recirculation rate of 2 m³/h can be achieved, resulting from the pump throughput and the filter set impedance: with this value, one full-volume recirculation can be carried on in about six days. LN₂ is used to cool the pump vessel, purifier cartridges and all the Ar transfer lines.

Two-phase nitrogen coming from thermal screen, together with nitrogen employed in GAr/LAr recirculation, is sent back to a \sim 1 m³ phase separator connected to two 30 m³ liquid nitrogen storages, filled up to about 80%. All the residual nitrogen gas produced in the various processes was converted back into liquid by a dedicated re-liquefaction system. This was designed to work in closed loop for safe operation in confined place; however operation in open circuit, with liquid nitrogen delivery by trucks, was also foreseen in case of prolonged emergency stops of the apparatus. The re-liquefaction system consists of twelve Stirling [36] Cryogenics BV SPC-4 (4-cylinder) cryo-coolers, delivering 4.1 kW of cold power each at 84 K with a nominal efficiency of 10.4%. The units operate independently, and automatically switch on/off to keep the nitrogen pressure at a fixed point, thus only delivering the actual cold power needed by the system.

Such required cold power can be determined by the consumption due to the insulation losses (heat input through joints, cryostat feet and cables), the nitrogen screen cooling (circulation pump and distribution lines) and the GAr/LAr recirculation-purification systems. During steady-state operations the cryogenic plant performed very well, successfully undergoing several safety, efficiency, redundancy tests and it demonstrated stability over the whole operating period. The average request of cold power was around 24 kW, mainly due to insulation losses. This was largely within the capability of the re-liquefaction system, as on average never more than 10 of the twelve Stirling units were found operational simultaneously.

The capability of the cryogenic plant allowed also performing a smooth detector commissioning: in order to ensure an acceptable initial LAr purity, the cryostats were evacuated to a pressure lower than 10⁻⁴ mbar, before commissioning. Vacuum phase lasted for three months, after which the cryostats could be cooled down to a temperature of 90 K within 7 days from start. Finally filling phase took place, lasting about two weeks, with the use of commercial LAr, pre-purified in-situ before being injected in the detector, at a rate of \sim 1 m³/hour/cryostat.

During the whole period the GAr recirculation was operating at maximum speed to intercept outgassing from the inner walls. One month after filling, LAr recirculation and purification was started on both cryostats.

Operations at LNGS demonstrated the very high reliability of the existing cryogenic plant, in particular for what concerns argon purification and stability of the system. As a matter of fact it was clearly shown in [15] how, for most of the data taking period, argon purity could be kept at a level corresponding to a free electron life-time higher than 7 ms. Furthermore at the end of the LNGS run the value of 16 ms (increasing) was reached, thanks to the use of a new recirculation pump that was tested in one of the two modules (for details please refer to [15], and see Fig. 18 below).

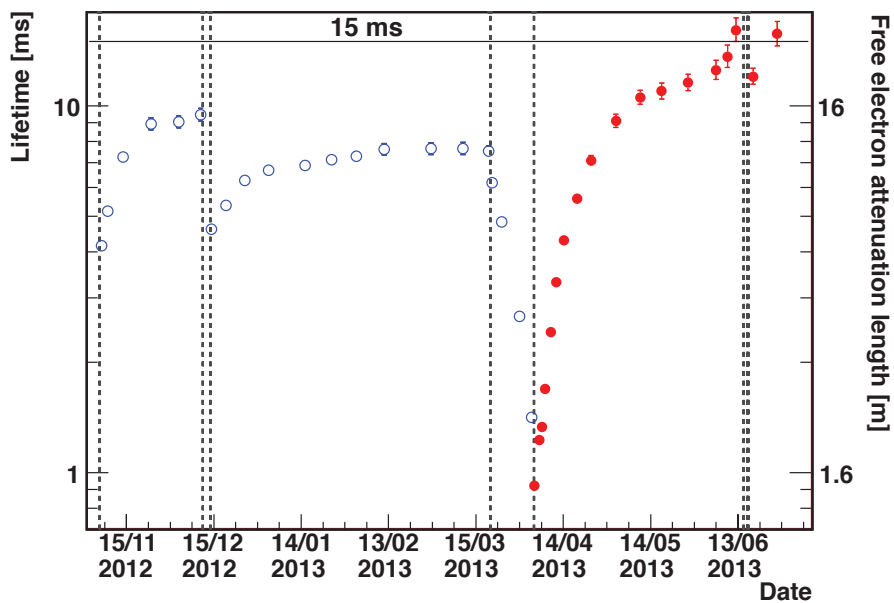


FIG. 18: Detail of the LAr purity in the East module of the T600 detector, as measured in the last months of operation. The high value of the electron life-time can be appreciated, as well as the ever-increasing trend in the last days of data taking achieved with a new model of circulation pump. Drops in purity correspond to stops of the recirculation for pump maintenance/substitution.

Other cryogenic parameters affecting the LAr-TPC performance were also accurately monitored during steady-state detector operations. In particular, the internal temperature in the two modules, directly connected to the electron drift velocity, was found to be stable and uniform at a level better than 0.25 K, well within the requirements (see Fig. 19). The same behavior was confirmed by the data on the internal absolute pressure (see Fig. 20): a very high stability was measured, with variations contained within around 10 mbar, far lower than those of ambient pressure, despite various stops of the recirculation system due to pump maintenance.

In general, the cryogenic system of the T600, repeatedly pre-tested against different types of emergencies, performed very well during operations in limiting conditions (deep underground location), and it allowed obtaining unprecedented results on argon purification. This result largely justifies the decision of carrying most of the plant and its design on to the next stage of the detector life within the Fermilab SBN program (see details in Section VD).

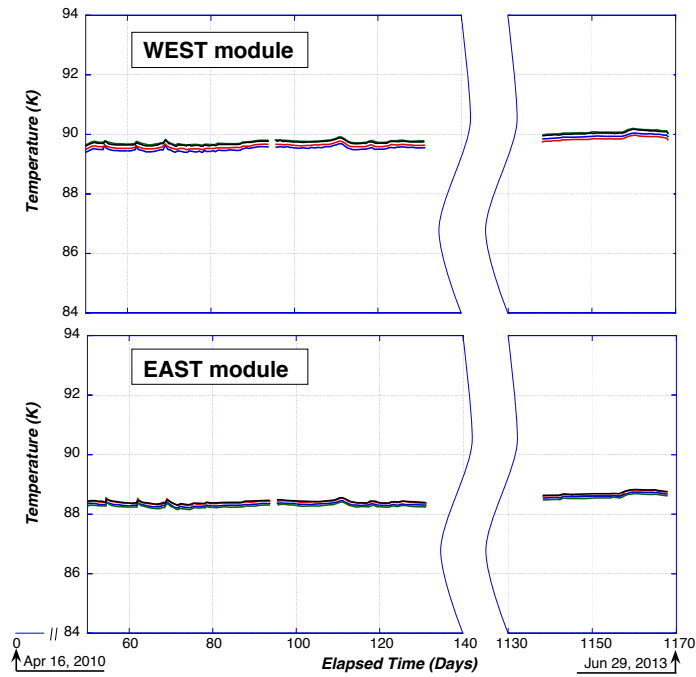


FIG. 19: Trend of the temperature in the two modules, measured in three different positions (bottom, middle height, top) during two periods of the LNGS run, one at its beginning in 2010, and the second in 2013, close to the end of data taking.

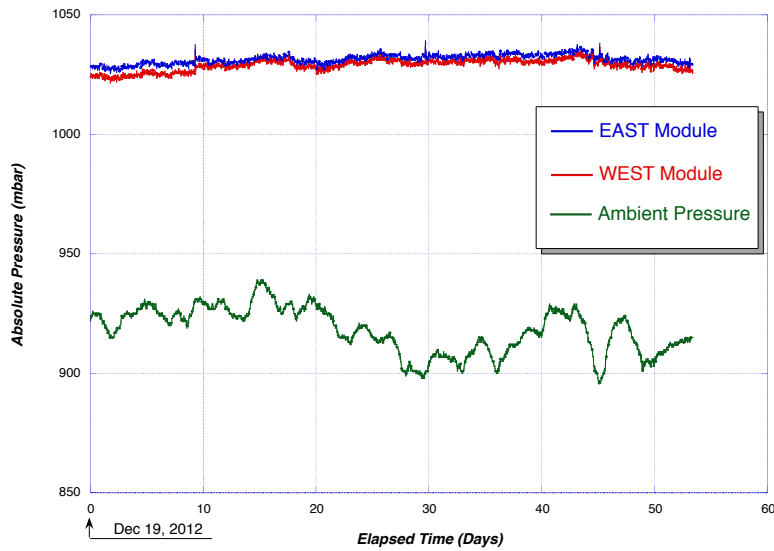


FIG. 20: Absolute internal pressure in the two modules during a two-month period between the end of 2012 and the beginning of 2013. Data can be compared with the trend of ambient pressure.

V. OVERHAULING OF THE T600 DETECTOR: WA104

The ICARUS-T600 detector has been moved to CERN for a complete overhauling, preserving most of the existing operational equipment, while upgrading some components with up-to-date technology in view of its future non-underground operation. The refurbishing (CERN WA104 project) will include the following main activities:

- substitution of the present cathodes with new ones of improved planarity;
- implementation of a new light collection system, to allow a more precise event localization and disentangle beam events from the background induced by cosmic rays;
- implementation of new readout electronics;
- other internal TPC updating: slow control system and cabling;
- realization of new vessels for LAr containment and new thermal insulation, based on a similar technology, as foreseen for LBNF and the SBN Near Detector;
- complete review and maintenance of the cryogenics and purification systems.

The transfer of the two T600 TPCs to CERN has been already completed: after the positioning of the first module into its transport vessel (see Fig. 21, Fig. 22 and Fig. 23), the first cargo has arrived to CERN at the middle of November 2014 (see Fig. 24). Movement operations at LNGS proceeded smoothly, with 4 to 6 people continuously involved for three weeks during October 2014. After the arrival of the second transport vessel at LNGS in November 2014, also the second T600 TPC was moved to CERN, being on site at the middle of December 2014.



FIG. 21: *Transport vessel positioning in front of the TPC at LNGS.*

All overhauling activities will be carried on at CERN building 185, which has been outfitted accordingly, with all necessary services (e.g. electrical, ventilation, heating, air recirculation in clean room). A dedicated clean room, to house the TPCs during operations, has been already completed (see Fig. 25). Since December 19th 2014, the first transported module is inside the clean room, while the second one has been stored inside the building (see Fig. 26)

This Section is organized as follows: Par. VA describes the main modifications of the ICARUS-T600 internal detectors. Par. VB shows the new layout of the Light Collection System, while the Electronics and DAQ in the FNAL configuration are described in Par. VC. Finally, Cryogenics and Purification new systems are presented in Par. VD.

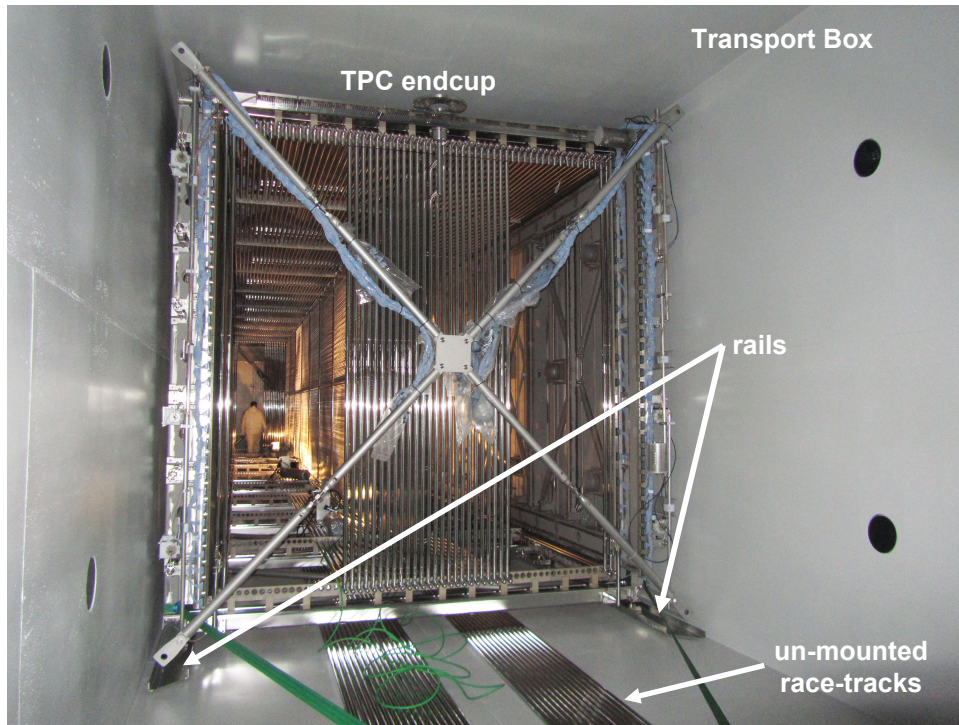


FIG. 22: *Start of movement of the TPC inside the transport vessel.*



FIG. 23: *The transport vessel on its way to CERN.*

A. TPC modifications

Minor changes are expected to be implemented, for what concerns the T600 TPC internal structure, with respect to the present configuration.

Distortions in the uniformity of the electric field in the drift volume of the T600, due to



FIG. 24: *The transport vessel in front of building 185 at CERN.*



FIG. 25: *Left: clean Room implemented inside CERN building 185, adapted for the T600 overhauling. Right: sketch of the Clean Room housing the T600 TPCs.*

positive ion charge accumulation induced by cosmic rays, have been investigated within the ICARUS collaboration. According to our estimates for ICARUS at shallow depths, the effect could be at most of a few mm, in agreement with the data collected in the 2001 technical run on surface in Pavia. To correct these distortions by making the electric field more uniform, some additional widely spaced shaping wire planes could be installed inside the sensitive volume, at the voltage of the potentials of the field cage electrodes. For instance, two arrays of wires (with a pitch of the ~ 10 cm) at 50 cm and 100 cm from the HV plane, anchored to the corresponding two field cage electrodes, could reduce the field distortion by almost an order of magnitude.

Moreover, small deviations from the linearity of the drift field have been found in the region close to the cathode plane on both modules. This is due to the not perfect planarity of the cathodes, owing to their pierced structure. This was confirmed by visual inspection after the

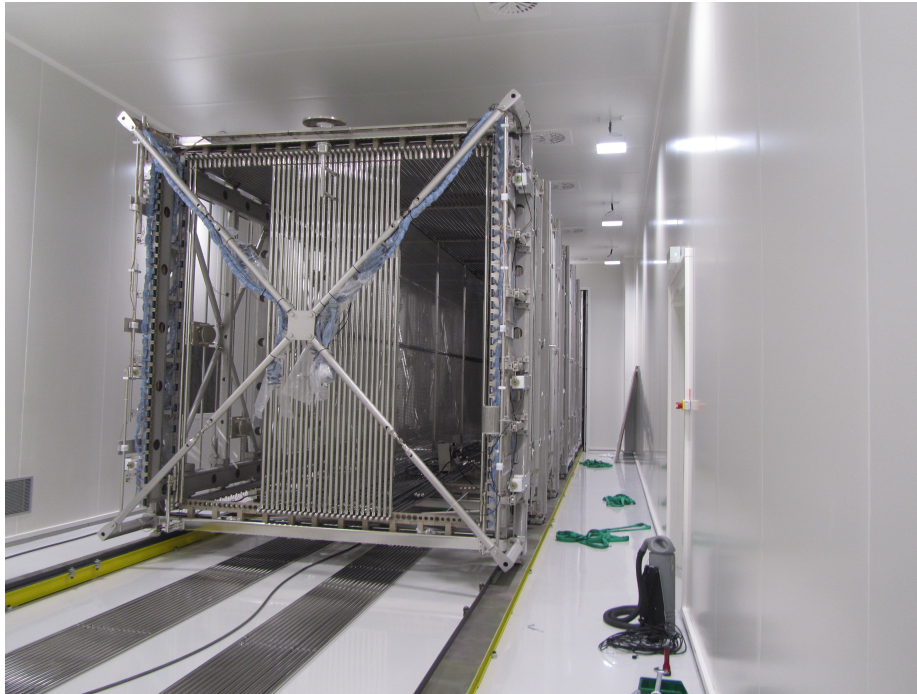


FIG. 26: *The first transported module inside the clean room at CERN.*

first cryostat opening in October 2014, where displacements from planarity of the order of 5 mm were found. Thus, in view of the SBN experiment at FNAL, it has been decided to change the present cathodes with new ones of improved planarity. The cathode surface could be either opaque or transparent to the scintillation light, depending on the request to perform the coincidence of the light signals from the two PMT arrays at either sides of the cathode. The detailed design of the new cathodes is currently under completion. Other activities on the T600 TPCs concern the updating of the slow control system for temperature, pressure and cryostat wall deformation monitors, as well as the design of new cabling for internal wires, PMTs and slow control sensors.

B. New Light Collection System Layout and Implementation

The future operation of the ICARUS LAr-TPC at the FNAL BNB at shallow depths requires an improved light collection system, able to detect with full efficiency the prompt scintillation light from events with energy depositions down to ~ 100 MeV.

The renovated T600 photo-detector arrangement should again collect the VUV scintillation signal which is present in the LAr simultaneously to the ionization, converting it to visible light.

The detection process in the LAr-TPC is initiated by the trigger signal opening a long “imaging” readout window, in which tracks are recorded in a time sequence, collected serially by the readout planes, while the electrons travel towards the end of the drift path. The full image of the event is therefore progressively extracted from the drift time distributions and from the many readout wires.

As already mentioned in Sec. III, the fast scintillation light signal in LAr must be put in coincidence with the $1.6 \mu\text{s}$ beam trigger gate, giving the huge rate of $\sim 0.83 \times 10^6$ c/y. Moreover, during the long duration of each readout window, there will be on average 44 cosmic

ray-induced scintillation light signals spread over the whole T600, four times the number of the cosmic tracks in a single TPC (accounting for the cathode transparency and because the time interval during which a light signal can be linked to a charge deposition is twice the maximum drift time).

The new light collection system has to be able to localize the track associated with every light pulse along the 20 m of the longitudinal detector direction, with an accuracy better than 1 m, which is smaller than the expected average spacing between cosmic muons in each TPC image.

In this way, the light collection system would be able to provide unambiguously the absolute timing for each track; and to identify, among the several tracks in the LAr-TPC image, the event in coincidence with the neutrino beam spill. The time accuracy of the incoming event with the new light collection system is expected to be at 1 ns level, allowing the exploitation of the bunched beam structure, lasting 1.15 ns (FWHM \sim 2.7 ns) every 19 ns, to reject cosmic events out of bunch as described in a SBN note [30]. An overall time resolution of 1.3 ns would then allow a background reduction of a factor \sim 4 by rejecting cosmic events occurring outside the RF buckets with a 2σ accuracy.

1. Tests on new cryogenic PMT models

The baseline solution for the T600 photo-detection system will rely on large surface Photo-Multiplier Tubes with hemispherical glass window of 200 mm (8") diameter, manufactured to work at cryogenic temperature. First tests were carried out to choose the most suitable PMT model. Three new large area PMTs, Hamamatsu R5912 Mod and R5912-02 Mod, and ETL 9357 KFLB, have been characterized both at room and at cryogenic temperature [37].

Tested PMTs have a borosilicate glass window and a bi-alkali photo-cathode (K_2CsSb) with platinum undercoating, to restore the photo-cathode conductivity at low temperature. Hamamatsu R5912 Mod and R5912-02 Mod PMTs have 10 and 14 dynodes, respectively, while the ETL 9357 KFLB has 12 dynodes. Photo-cathode uniformity, gain, linearity, dark count rate and Quantum Efficiency (QE) for LAr scintillation light have been measured.

For gain, linearity and uniformity measurements, PMTs were illuminated with a 405 nm NICHIA NDV1413 laser diode, using an Avtech AVO-9A-C-P2-LARB pulse generator and an optical fiber (7 μ m core diameter, 3 m long). An appropriate support was used to maintain the fiber in a fixed orientation, normal to the PMT window, while allowing to move it in various positions on the window itself. A CANBERRA 2005 pre-amplifier and an ORTEC-570 amplifier were used to form PMT signals, then acquired with an ORTEC-Easy-8k,12 bit Multi Channel Analyzer. PMTs dark count rate has been measured with a different acquisition system, i.e. with a CAEN V812 discriminator and a CAEN V560 counter. The discrimination threshold was gradually increased from 1 to 255 mV, with 1 mV steps.

To test them at cryogenic temperature, the PMTs were directly immersed in liquid nitrogen ($T = 77$ K), to simulate real experimental conditions. Measurements were carried out after a couple of days of rest in the cryogenic bath. The same setup and acquisition system described above were used, with the fiber and the other cables allowed to enter by a proper feed-through, used to preserve darkness conditions and thermal insulation (see Fig. 27).

Hamamatsu PMTs showed a good uniformity, within 10%, up to 10 cm from the tube axis, where a gain reduction occurs, probably due to the electric field non-uniformity in the peripheral region of the tube. While this behavior does not occur with ETL 9357 KFLB, lower uniformity is measured, \sim 20%; furthermore a very low signal has been measured in a specific region of the

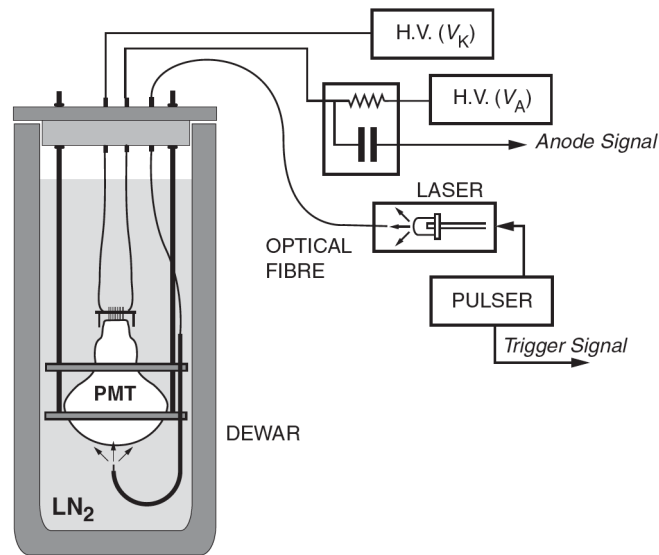


FIG. 27: *Experimental setup for the characterization of PMTs immersed in liquid nitrogen.*

photo-cathode for this model: this can be explained by a degradation of the photo-cathode for the specimen under test. Due to this problem and after discussions with the manufacturer, it was decided not to test the ETL 9357 KFLB at cryogenic temperature, pending further tests by the producer.

The gain of the devices was estimated from Single Electron Response (SER) as a function of the applied voltage and operating temperature. The gain reduction occurring at 77 K is evident for both Hamamatsu devices, being $\sim 70\%$ in the R5912 and $\sim 35\%$ in the R5912-02 with respect to room temperature data (see Fig. 29 Left). Hamamatsu R5912 MOD remains linear up to 400 phe, while R5912-02 MOD reaches again the saturation regime after a few photo-electrons, about only 10 phe.

In general both photo-detectors showed a good behavior and are suitable for cryogenic application.

A different experimental setup was used to measure the QE of the photo-cathodes in the VUV light region. To make them sensitive to VUV light, the PMT sand-blasted glass windows were deposited with a TPB coating of ~ 0.2 mg/cm².

The measured QE accounts then for: the shifting efficiency of the TPB, a geometrical factor (on average half of the photons will be re-emitted in the opposite direction with respect to the photo-cathode) and the QE of the PMT for blue light. As shown in Fig. 28, the PMT under test was placed inside a steel chamber optically connected to a McPHERSON 234/302 VUV monochromator.

The experimental setup included a McPHERSON 789A-3 scanner, a McPHERSON 632 Deuterium lamp, a rotating Al+MgF₂ mirror, an AXUV-100 reference photo-diode and collimating optics. The whole system was kept under vacuum, down to 10^{-4} mbar, to prevent ultraviolet light absorption. Thanks to the rotating mirror, the light spot was directed alternatively on the PMT surface or on the reference photo-diode. The QE was obtained by comparing the current measured with the PMT and the same collected with the reference diode, keeping the light constant. Measurements were carried out by means of a picoammeter. Results for LAr (128 nm) and LXe (165 nm) emission peaks are reported in Fig. 29 Right. ETL 9357 KFLB has, at 128 nm, a $QE = 4.7\% \pm 0.7\%$, while Hamamatsu PMTs present a higher value, $QE =$

$7.0\% \pm 0.6\%$.

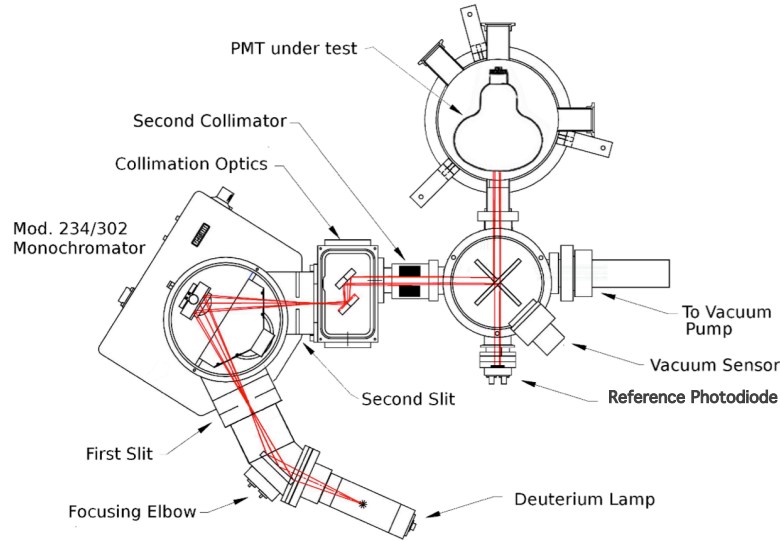


FIG. 28: *Experimental setup for the evaluation of the response of PMTs to the VUV light.*

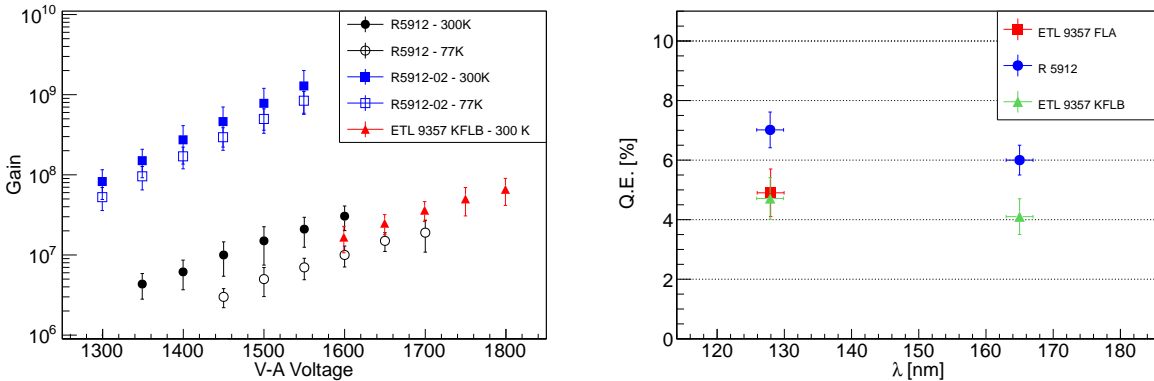


FIG. 29: *Left: gain trends for tested PMTs at room (full spots) and at cryogenic (empty spots) temperature as a function of the voltage between anode and cathode. Right: Quantum Efficiency of the tested devices at LAr emission peak (128 nm) and LXe emission peak (165 nm).*

2. New Light Collection System Layout

After the choice of the PMT model and the purchase of the devices, a careful evaluation of the performance of each PMT before its final mounting inside the T600 detector will be carried out. Measurements will be focused on the main PMT parameters which are temperature dependent, to isolate possible defects in the devices. In particular, the following features will be characterized: shape of the anode pulse, SER of the anode pulse, gain, single-electron transit time (spread, pre- and late-pulsing), after-pulses, dark-count rate and spectrum. To this purpose a test facility will be setup in a dedicated INFN laboratory.

PMTs will be located in the 30 cm space behind the wire planes with sustaining structures: the sustaining system will allow the PMT positioning behind the Collection wire planes according to the geometrical planned disposition. PMTs induce spurious signal on wire planes: to reduce this drawback, still under investigation, each PMT will be surrounded by an electrostatic shield. A drawing to show a 90-PMTs layout behind the wire planes is presented in Fig. 30.

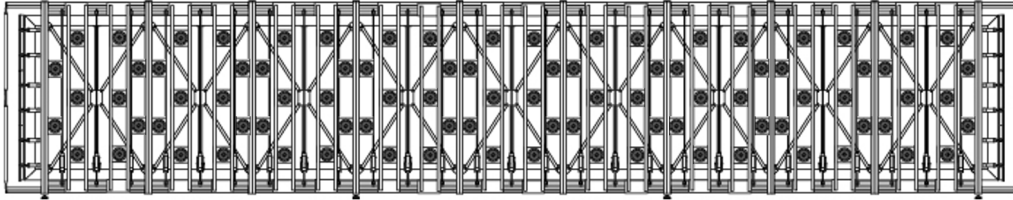


FIG. 30: Drawing showing a 90-PMTs layout behind the wire planes. PMTs are depicted as dark circles. This design yields a 5% photo-cathode coverage.

To prevent any impedance mismatch in the signal lines, PMT negative biasing will be adopted. This scheme will adopt two cable for each device, one for the DC HV power supply and one for the signal. The main disadvantage is the operation with photo-cathodes at HV voltage close to the collecting wire planes. Despite electric fields of about 600 V/cm are expected, the TPC electric field and the electron collection on the wire planes will be not altered. Moreover, the adoption of a fine-mesh grid in front of each PMT should avoid any interference between charge collection and light detection.

Fast waveform digitizers are required to exploit the bunched beam structure. 1 GHz waveform digitizers with zero suppression will be adopted, preventing the use of shaping pre-amplifiers; the input dynamics must permit the recording of the scintillation light fast component pulses and, at the same time, of the single photons arriving from the slow component de-excitation. A PMT timing calibration/monitoring system will also be implemented. The baseline solution consists of pulsed laser diodes and optical diffusors installed at various locations in front of the PMTs, possibly on the TPC cathodes. Short pulses (< 1 ns) of laser light will be transmitted inside each TPC, by means of optical fibers and feed-throughs, to each of the diffusors. This will allow the PMTs lighting with approximately uniform intensity. A dedicated R&D activity is foreseen to evaluate the timing performance of this system and to optimize the optical fiber feed-through implementation.

Dedicated calculations have been set up to evaluate the performance of the upgraded ICARUS light collection system, in terms of event localization for both cosmic muons and electromagnetic showers. Cosmic muon tracks in the active liquid argon volume are simulated as straight lines with directions distributed as $\cos^2 \theta$ around the vertical axis, where θ is the zenith angle. About 40,000 VUV photons/cm (corresponding to the amount of scintillation light from 2.1 MeV/cm energy deposition of a minimum ionizing particle in a field of 500 V/cm) are produced uniformly along the muon tracks and are emitted isotropically. Rayleigh scattering and the presence of delta rays in a 15 cm radius cylinder surrounding the muon path are also included in the simulation.

Electromagnetic showers are simulated as clusters containing single 1 MeV points ($\sim 21,000$ photons) up to the deposited energy. No reflection and diffusion on walls have been simulated, since the LAr VUV scintillation photons are absorbed by all materials. The number of detected photons is derived in terms of solid angle calculation.

To estimate the localization capability of the light collection system, a Monte Carlo simu-

lation has been carried out. For each simulated event the barycentre of the light emission has been calculated, by averaging on the coordinates of the PMTs and weighing on the different signal intensities. This was done both for the vertical and horizontal coordinates. The spatial resolution of the system, evaluated as the difference between the simulated track barycenter and the same quantity reconstructed as described above, is found to be better than half a meter, as shown in Fig. 31. This will allow to strongly narrow the LAr region in which to search for neutrino beam-induced events.

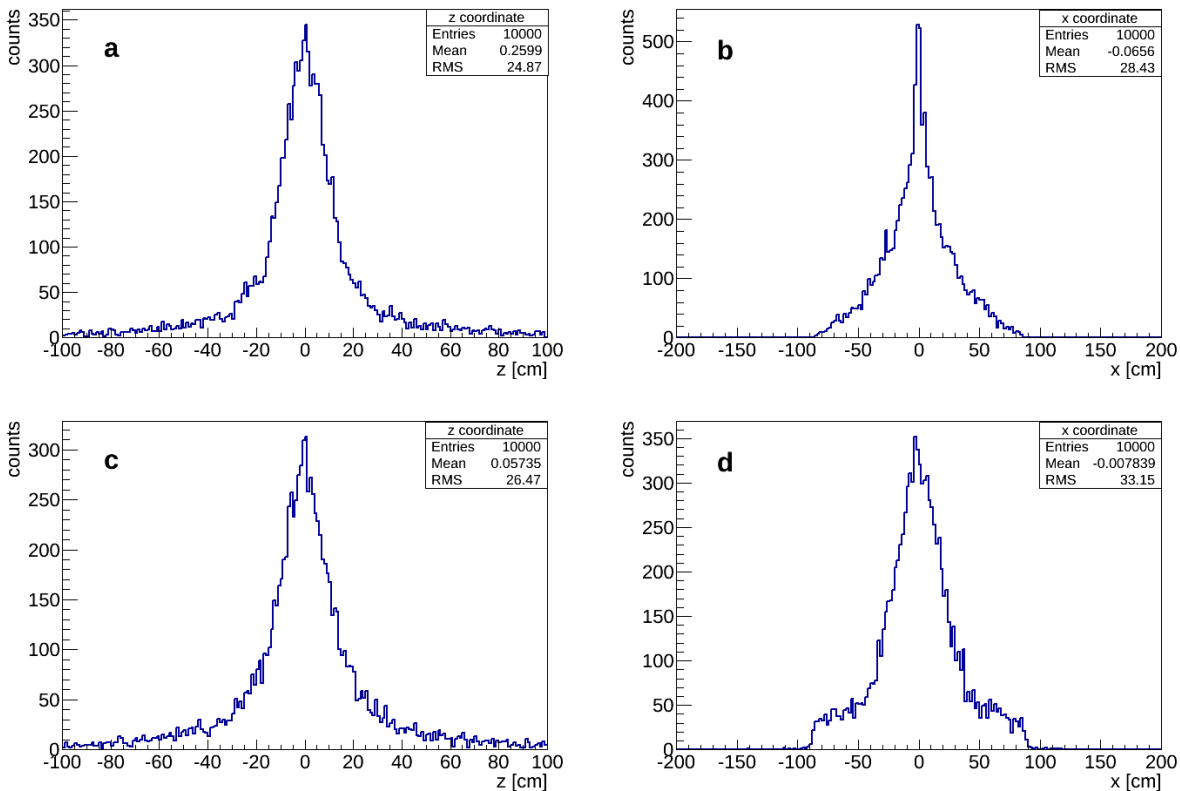


FIG. 31: Monte Carlo evaluation of the residuals from the correct position, both along the beam direction z and along the vertical coordinate x , for electromagnetic showers of about 200 MeV (a,b) and cosmic rays (c,d). In plot (d) the residual distribution is affected by the detector boundaries along the x coordinate.

C. New Electronics, DAQ and Trigger

1. Electronics

The ICARUS-T600 electronics was designed starting from an analogue low noise warm front-end amplifier followed by a multiplexed (16 to 1) 10-bit AD converter and by a digital VME module that provides local storage, data compression, and trigger information. The overall architecture, based on VME standard, was appropriate for the experiment, taking into account that the T600 electronics design started in 1999. The first production was carried out in 2000 and tests, at surface on the first T600 module, were successfully performed in 2001.

The present architecture (essentially a waveform recorder followed by circular buffers switched by trigger logic) is still valid, however possible improvements are now conceivable, taking advantage of new more performing and compact electronic devices.

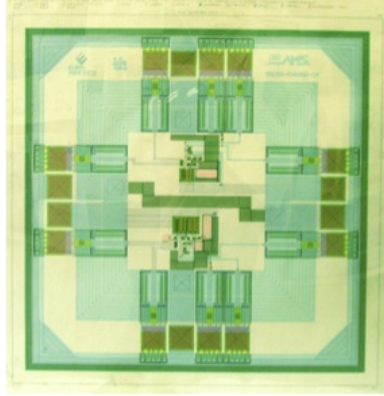


FIG. 32: *BiCMOS dual channel custom analog pre-amplifier.*

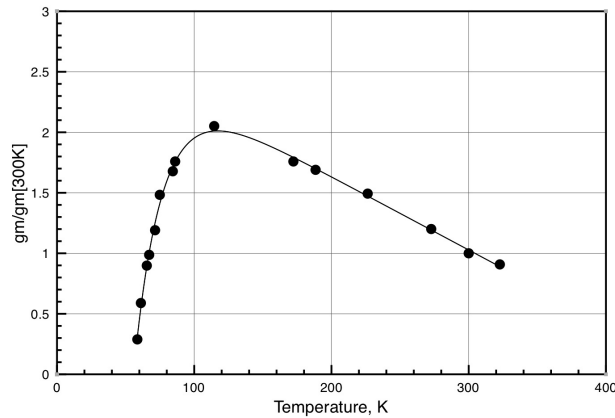


FIG. 33: *Typical variation of the input stage transconductance g_m with temperature for junction Fet.*

The analogue front-end amplifier, used in the T600 LNGS configuration, is perfectly adequate: the only proposed change is the adoption of a smaller package for the BiCMOS (see Fig. 32) custom amplifier, dual channel, which is already available. The possibility to have the front-end in LAr is also considered.

The amplifier serial input noise, e , linearly increases with detector and cable capacitance, C_d , and decreases with input stage transconductance, g_m :

$$e^2 = \frac{C_d^2}{g_m}. \quad (1)$$

Transconductance is 26% higher at LAr temperature (86 K), see Fig. 33, and, together with the reduction of cable length, an improvement of S/N is expected with cold amplifiers. However, in the case of large mass LAr-TPCs, a detector lifetime in the order of tens of years is expected. In this period, it is natural to foresee improvement programs in the electronics,

because of its constant evolution and progress. An architecture allowing for major and easy upgrading with an accessible electronics has been then chosen.

The gain of the front-end amplifier and filter is $\frac{1V}{164fC}$. The 10 bit ADC input range is 1 V, therefore the least count is equivalent to 1,000 electrons. This value matches with the amplifier noise of $\sim 2,000$ electrons, given a detector capacitance of 450 pF (signal wires plus cables).

The T600 run at LNGS on the CNGS neutrino beam confirmed a S/N better than 10 for m.i.p. on about 53,000 channels. A relevant change, in the new electronics design, concerns the adoption of serial ADCs (one per channel) in place of the multiplexed ones used at LNGS. The main advantage is the synchronous sampling time (400 ns) of all channels of the whole detector, not to mention compactness and price. A very reliable and cost effective new flange (CF200) has been developed for the T600 future operations, see Fig. 35 Left. The internal structure of a via in this CF200 flange is shown in Fig. 34. The external contacts, on both sides, not visible in Fig. 34, are on a different plane respect to the via, and allow for SMD connectors use. The white squares are brass disks that reinforce the flange structure, in order to stand atmospheric pressure without deformation in case of use in vacuum vessels.

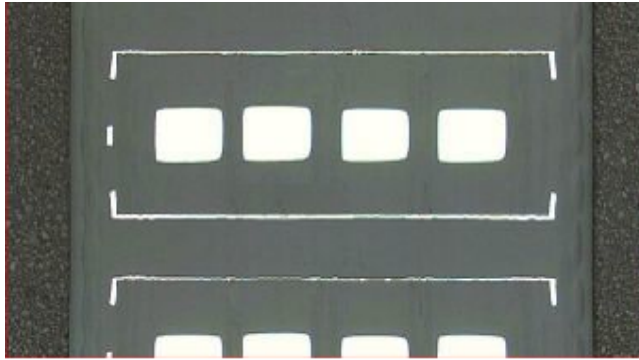


FIG. 34: Section of signal flange (5 mm): the copper via contact (white lines in the photo) is fully embedded in solid G10.

This flange allows the connection of 16 cables (512 channels), to exploit the external side of the flange as an electronics cards backplane in a special crate (Fig. 35 Right). The connectors on the external side allow for direct insertion of electronics boards, where both analogue and digital electronics, with a compact design, are housed.

In Fig. 36 the first working prototype board is shown. It serves 64 channels and uses serial optical links. The 8 boards of one flange may use the same serial optical link as it is shown in the block diagram of Fig. 37. The digital part is fully contained in a high performance FPGA (Altera Cyclone V) that allows easy firmware upgrading. Behind the FPGA, sockets for front-end amplifiers are visible together with the direct insertion connectors that convey wire signals. In Fig. 38 the pre-amplifiers are shown. The board is scored so the amplifiers will be snapped in eight sets of eight pre-amplifiers.

Performance, in terms of throughput of the read-out system, has been improved replacing the VME (8 - 10 MB/s) and the sequential order single board access mode inherent to the shared bus architecture, with a modern switched I/O. Such I/O transaction can be carried over low cost optical Gigabit/s serial links.

As mentioned before, the cold electronics option could be considered, provided a suitable design is found. The ICARUS collaboration does not have a ready-to-use cold pre-amplifier, even if in the past many tests, eventually abandoned, were carried out for this solution [38]. If

such cold pre-amplifier is found, one should adapt a pre-amplifier board inside the cold vessel, close to the wire support, modulo 32 or 64, and substitute the piggy back 8-channel amplifier boards, described before, with suitable receivers, maintaining the digital part as it is and the 400 ns sampling time.

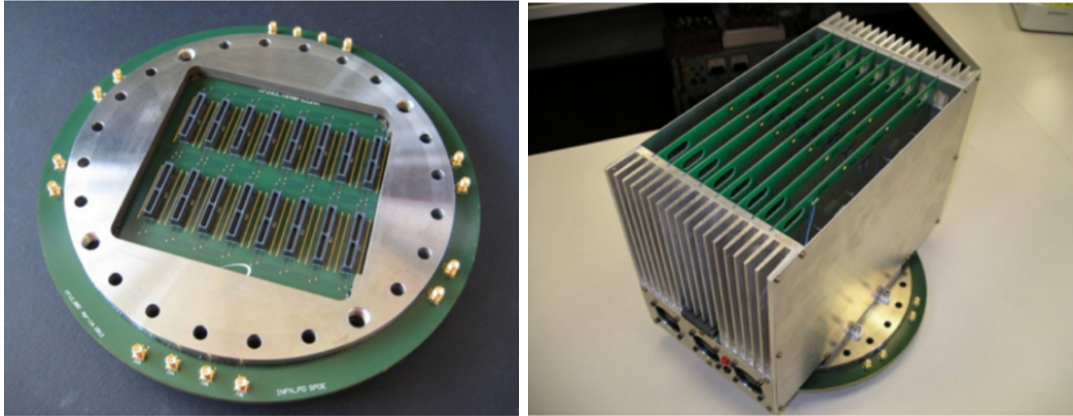


FIG. 35: *Left: the new T600 flange without the cards cage. Right: the new T600 flange with the cards cage and 8 boards inserted without front panels.*

2. Trigger and DAQ

The trigger system of the T600 detector will exploit the coincidence of the prompt signals from the scintillation light in the LAr-TPC, recorded by the PMT system, with the proton spill extraction of the BNB within a $1.6 \mu\text{s}$ gate.

PMT digitized pulses are sent to a front end dedicated board to be processed by FPGA modules, requiring a logic on multiple PMT signals for the generation of the trigger. Discrimination thresholds have to be set to guarantee the detection of all the event associated to each neutrino interaction with energy $E > 100 \text{ MeV}$.

The PMT trigger signal will be then sent to the T600 Trigger Manager, where it will be combined with the time information from the beam spill to initiate the readout of all the TPCs. A multi-buffer event recording will be adopted with a 3-level veto, as for the CNGS beam exploitation, able to give different priorities to different trigger sources, thus minimizing DAQ dead-time. The system, similar to the LNGS run one described in Sec. IV C, will consist of a Real Time (RT) controller and FPGA boards, communicating with the DAQ in handshake mode. The RT controller will monitor the number of available buffers in the digital boards, preventing the generation of new triggers in case they are full. The FPGA boards will implement time critical processes, like the opening of Booster Beam gate and the time stamp of each trigger. FPGA boards are also expected to record the trigger source and mask, to monitor the trigger rates and to control the overall system stability. The T600 Trigger Manager will also allow combine in the trigger logic the signals coming from the new cosmic ray tagging system (see Sec. VI).

At the nominal BNB intensity of 5×10^{12} pot/spill, ~ 1 neutrino interaction, either charged or neutral current, every 180 spills is expected to trigger the T600 detector at the far position with vertex in the LAr-TPCs (1 neutrino every 240 spills considering charged currents only). A slightly lower trigger rate, one every 210 spills, will come from beam-associated events; the



FIG. 36: *First working new electronics prototype board.*

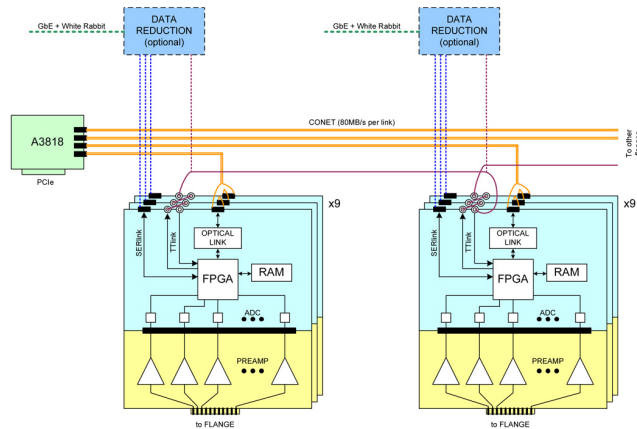


FIG. 37: *Arrangement of the read-out boards on different flanges.*

dominant trigger source, 1 over 55 spills, is expected from cosmic rays. Globally, about 1 event every 10 s is foreseen in the T600 LAr-TPC at the standard 4 Hz repetition rate of the Booster Neutrino Beamline. This ~ 0.1 Hz trigger rate is well within the 50 MB/s DAQ throughput already realized for the CNGS data taking at LNGS. Actually, the significant improvement in the readout throughput achievable with the new serial optical links will ensure an even better

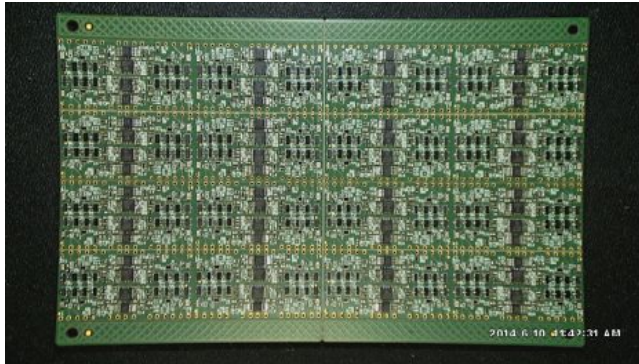


FIG. 38: 64 front-end amplifiers before snapping in 8 sets of 8 amps.

performance. Therefore, the present DAQ is largely adequate to operate without dead-time not just with the standard 4 Hz repetition rate of the Booster Beam, but also up to the ~ 15 Hz maximum repetition rate.

Provided that a precise beam extraction signal is available, the trigger and DAQ system is also well suited to the exploitation of the bunched beam structure, accounting for the 1 GHz sampling of the PMT waveforms and the precise spatial reconstruction of the neutrino interaction vertex in the TPCs. The excellent performance in event timing achievable with the ICARUS-T600 detector has been proven by the precision measurement of the neutrino velocity on the CNGS beam [13, 14]. This result relied mainly on:

- the waveform of the extracted proton beam time-structure signal, recorded at CERN with a 1 GHz sampling triggered by the kicker magnet signal;
- an absolute GPS-based timing signal, distributed by LNGS laboratory to the ICARUS-T600 detector via a ~ 8 km optical fiber, synchronized with the CERN absolute timing within few ns;
- the waveform of the PMT trigger signal recorded with a 1 GHz sampling;
- the evaluation, with ~ 1 ns accuracy, of the time corrections corresponding to the distance of the event from the closest PMT and the position of the interaction vertex along the ~ 18 m of the detector length. Note that the time corrections also include the contribution of the PMT transit time, different for each device.

A similar strategy could be adopted at FNAL as well, if the waveform of the fine bunched structure of the Booster beam will be provided with ~ 1 ns resolution. As a further simplification, a precise matching of the neutrino interaction in the T600 active volume with the corresponding bunch could be obtained without need for an absolute timing, if the beam extraction signal will be delivered directly to the T600 detector exploiting the recently developed White Rabbit timing protocol [39].

D. New Cryogenic and Purification systems

The SBN program provides a first opportunity for the CERN and FNAL engineering groups to collaborate on the design of LAr-TPC infrastructure. Once established, this collaboration

could have a significant impact on designs for other short and mid-term projects leading to a long-baseline neutrino facility. While most of the components of the T600 detector will be reused after overhauling at CERN, the LN₂ delivery system is expected to be replaced and a completely new cryostat and cryogenic layout will need to be developed. The following describes the cryostat and cryogenic needs for the Far Detector.

New cryostats will host the refurbished T600 detector. LAr will be contained in two mechanically independent vessels, of about 270 m³ each. According to the past experience, to efficiently outgas the internal surfaces and obtain an appropriate LAr purity, the cold vessels must be evacuated to less than 10⁻³ mbar. Therefore the vessels need to be tight to better than 10⁻⁵ mbar l s⁻¹. The new T600 vessels will be parallelepipedal in shape with internal dimensions 3.6 (w) × 3.9 (h) × 19.6 (l) m³. Aluminum welded extruded profiles (see Fig. 39) will be employed, designed in collaboration with industries and Milano Politecnico (Italy): they are requested to be super clean, vacuum-tight and to stand a 1.5 bar maximal operating internal overpressure. Executive design for both the profiles and welding (mounting) procedures has already been procured: further details are shown in Fig. 43, Fig. 44 at the end of the section.

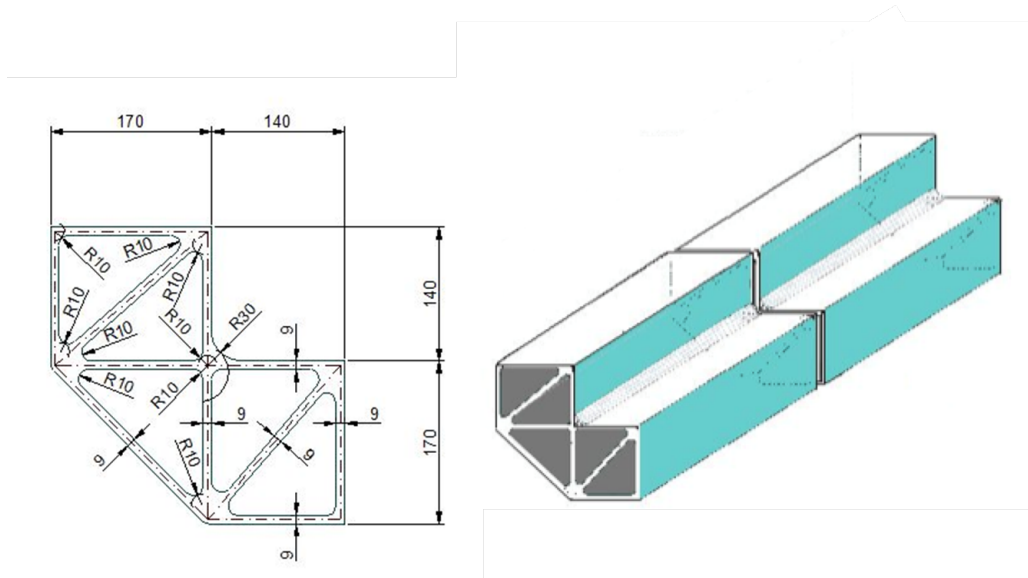


FIG. 39: Detail of an aluminum extruded profile corner, 2D and 3D. More drawings are shown at the end of the section.

Such new solution represents a significant simplification with respect to the aluminum honeycomb used in the LNGS run, whereas it implies a slight increase in the cryostat weight, 30 t each. Use of aluminum LAr vessels is also particularly attractive as it offers very good shielding against external electronic noises, and it provides large thermal conductivity that improves the temperature uniformity inside the LAr. As in the LNGS run, walls are double-layered and can be evacuated, leading to efficient leak detection and repair.

The cold vessels will be enclosed inside a common heat exchanger (thermal shield) in which two-phase (gas+liquid) nitrogen is circulated. As in the past run, a mass ratio less than 5:1 will be kept between the liquid and the gas phases, which ensures temperature uniformity all along the shield.

A purely passive polyurethane foam is chosen for insulation, based on the membrane tanks technology. This technique has been developed for 50 years and is widely used for large industrial storage vessels and ships for liquefied natural gas [40, 41]. The solution has been adapted to the ICARUS design by the GTT firm, and it is similar to the one to be used for the membrane cryostat of the Near Detector. In Fig. 40 and Fig. 41 details of the insulation elements and expected thermal gradients respectively are shown, as an example. In Tab. II the thermal flux through the various elements is listed. An insulation thickness of 600 mm will be used for the bottom and lateral sides; for the top-side a maximum thickness of about 400 mm will be used. With this configuration, the expected average thermal losses will be of around 10 W/m^2 , resulting in a heat loss through the insulation of $\sim 6.6 \text{ kW}$. All the external heat contributions (cables, pumps, transfer lines, etc.) can be accounted for a value not exceeding 5.4 kW , leading to a total heat load of about 12 kW .

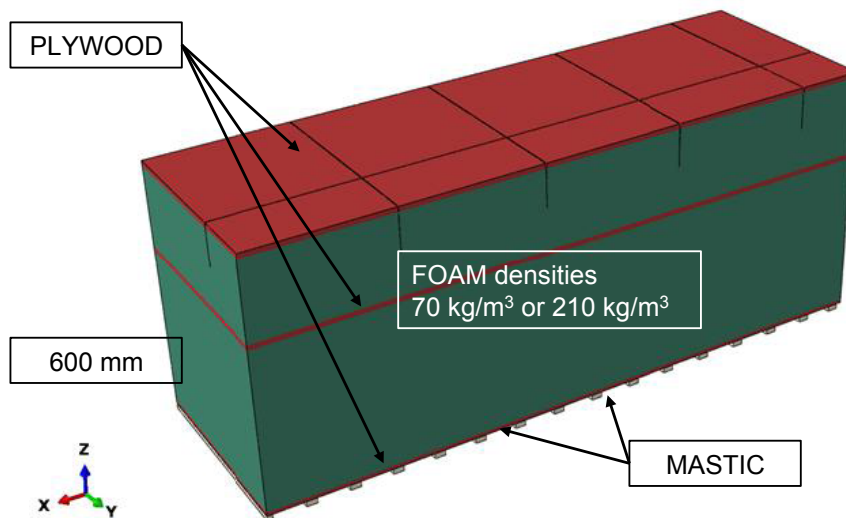


FIG. 40: 3D model of the newly-proposed T600 insulation. 600 mm element displayed

Panel thickness (mm)	Foam density (kg/m^3)	Total heat (W)	Surface (m^2)	Thermal flux (W/m^2)
400	70	7.800	0.750	10.40
400	210	13.530	0.750	18.04
600	70	5.200	0.743	7.00
600	210	9.026	0.743	12.15

TABLE II: Thermal flux through the insulation elements, as a function of thickness and foam density, from GTT study. The foam density will be usually of 70 kg/m^3 , while amounting to 210 kg/m^3 in correspondence to the feet of the detector.

The Far Detector renovated cryogenic design is being developed, wherever possible, with a focus on commonalities with the Near Detector one, to be used across both experiments and also as a stepping stone for LBNF collaborative efforts. With this idea in mind, this system

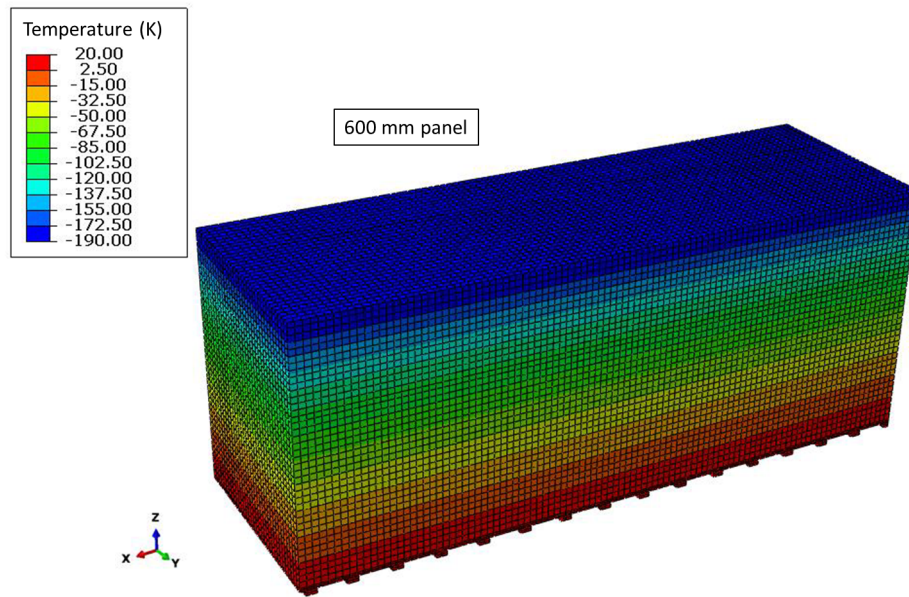


FIG. 41: *Finite elements study of the thermal gradient in the 600 mm thick element. Note that on this picture ambient temperature is on the lower side of the element*

is expected to be modular in design, able to be enlarged for future projects, and portable, i.e. constructed on skids that can be tested separately, prior to delivery to FNAL for installation.

The original scheme of ICARUS-T600 cryogenics and LAr purification systems will be preserved, and most of the present plant, INFN property, will be reused. In the same way, the requirements will remain the same, with respect to the past, as described in Sec. IV D.

One main difference, with respect to the previous LNGS run, will be in the logistics, due to the different location of the detector (at shallow depths). If further updates were needed, they would be carried on by the hosting laboratories, following the specification given by the ICARUS Collaboration. On the other hand, during the different stages of the program (overhauling and, later, commissioning and data taking) it will be responsibility of the hosting laboratory to conceive and take care of the necessary maintenance of circuitry and control systems. The same goes for what concerns the plants-related logistics.

At Fermilab, the cooling circuit will be operated in open loop: the Stirling re-liquefaction will not be used. Fig. 42 shows once again the existing cryogenic system on the ICARUS-T600 detector, this time highlighting the Stirling re-liquefaction system that will be discarded with the implementation of the open-loop LN₂ delivery system.

Further discussions on specific technical aspects of the cryogenic system are underway, mainly regarding the purification system (filters), best re-condensation strategy, ullage conditions. However, given the already discussed very successful operation of the existing plant (see Sec. IV D), the ICARUS Collaboration intends to maintain the choices made in its previous experience, with the exceptions described above, and carry them on to the coming SBN program at FNAL.

The envisioned schedule for the development of the ND/FD cryogenic systems is related to the request to have the Near and Far Detectors ready for commissioning in fall 2017, with data taking starting in April 2018. LAr Cryogenics groups are being formed both at CERN and

FNAL, and are set to collaborate to meet the goals.

Fig. 42 shows once again the existing cryogenic system on the ICARUS-T600 detector, this time highlighting the Stirling re-liquefaction system that will be discarded with the implementation of the open-loop LN₂ delivery system.

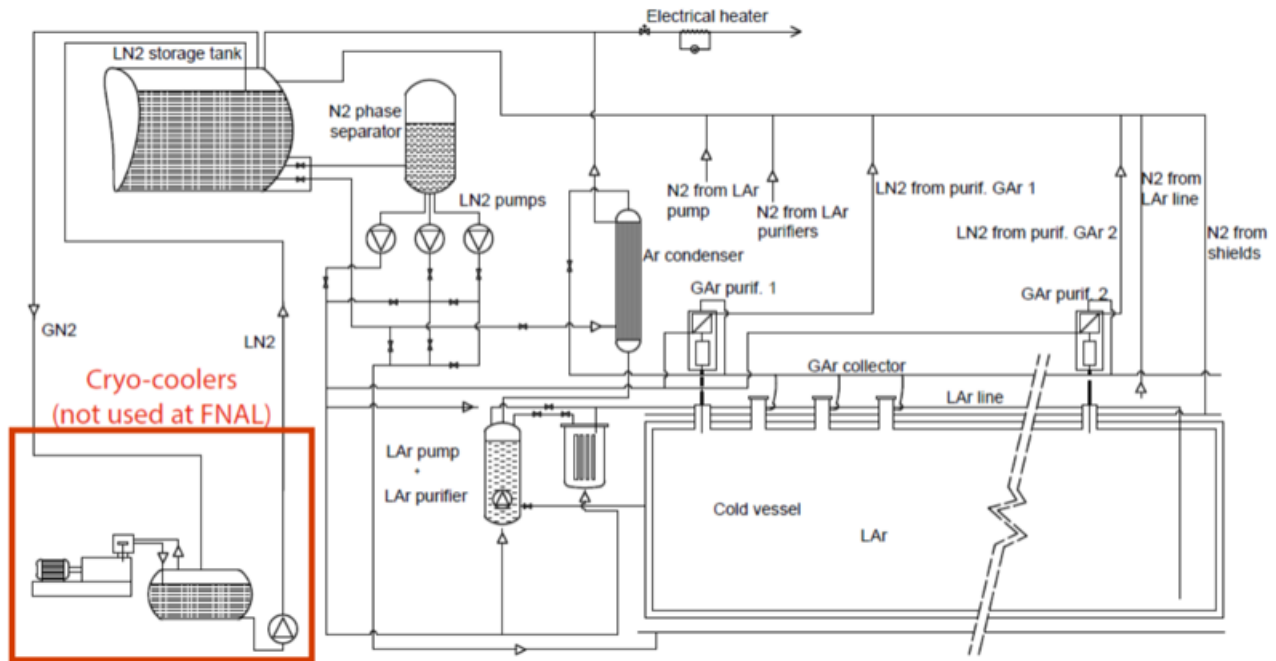


FIG. 42: Schematic diagram of the existing T600 cryogenic system, which will be maintained during the FNAL operations as well. The highlighted section in the lower left represents the old Stirling re-liquefaction units, which will be replaced by a new open-loop LN₂ delivery system.

The ICARUS-T600 detector is expected to be delivered to FNAL in the first half of 2017, with about 6 months needed for installation. Commissioning can take place during the second half of 2017. It will require from 3 to 5 months, based to the experience gained at LNGS. In Gran Sasso 5 months were needed, including about 3 of vacuum pumping. The consumption of LN₂ and LAr during this commissioning phase can be estimated, based on the fact that the total expected heat loss through the new insulation, as mentioned above, is of the order of 10 kW, and that larger cold power consumption during the first cooling down can be assumed. Approximately 100,000 liters of LN₂ should be needed for cooling down, along with 273,000 liters of LAr per module of the T600. Assuming present pricing for the cryogenic liquids, Tab. III can be constructed, summarizing the estimated costs of LN₂ and LAr for the commissioning phase.

Before closing this section, further drawings of the new cold vessels are reported, referring as an example to one of the endcaps of the vessel, exploded (Fig. 43), and to the whole exploded view (Fig. 44), respectively.

Material	Quantity (l)	Price(US\$)/liter	Total cost (US\$)
Liquid nitrogen	100,000	0.07	7,000
Liquid argon (per module)	273,000	1.5	409,500
Total*			826,000

TABLE III: Summary of costs of the commissioning phase, for what concerns usage of LN_2 and LAr during cooling down. *Note that Liquid argon cost is detailed for one module of the T600, while the grand total accounts for both modules ($2 \times 409,500$).

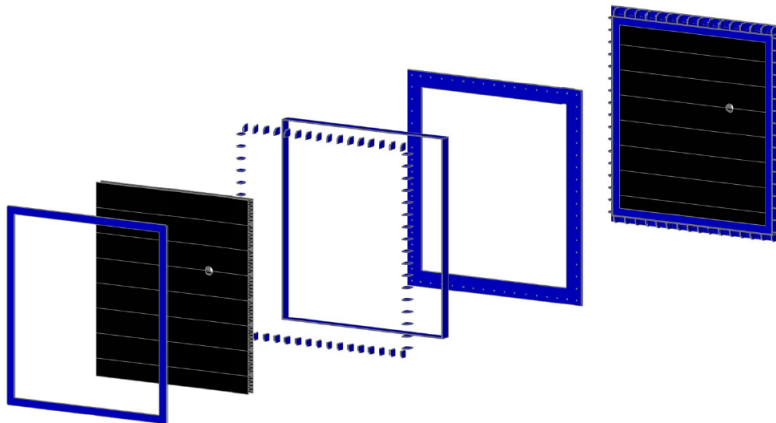


FIG. 43: Exploded detail of one of the endcaps of the new aluminum vessel. The hole corresponding to the LAr extraction line (for liquid recirculation) is visible.

VI. COSMIC RAY TAGGING SYSTEM

As already mentioned in Sec. III, very effective new methods must be introduced to reduce the cosmic ray related signals [29]. For example, a segmented, fast anti-coincidence with 4π coverage detector (Cosmic Ray Tagging System, CRTS), may record each charged particle crossing the outer boundaries of the LAr containers. At the nominal BNB intensity of 5×10^{12} pot/spill, only 1 neutrino CC interaction every 240 spills is expected to trigger the T600, with vertex in the LAr -TPCs. This rate has to be compared with the expected cosmic rays rate of 1 every 55 beam spills. The CRTS detector could be used to deplete by a significant factor the spurious cosmic ray induced interactions, by tagging events in the beam spill without any crossing cosmic ray. According to the expected time resolution of the PMT detection system and of the CRTS, a tagging window <100 ns will reduce spurious coincidences generated by CRTS.

The positions and the timings of all random muon tracks crossing the walls of the CRTS during the T600 imaging window will be recorded. Each muon track reconstructed in the TPC may be then correctly determined by associating the charge image with the corresponding absolute drift time t_0 coming both from the CRTS and from the internal light collection system, matching the track geometry with the CRTS recorded positions.

This would be achieved by means of a system which provides signals, independently from the LAr -TPC and the light collection system, that indicate the passage of charged particles through

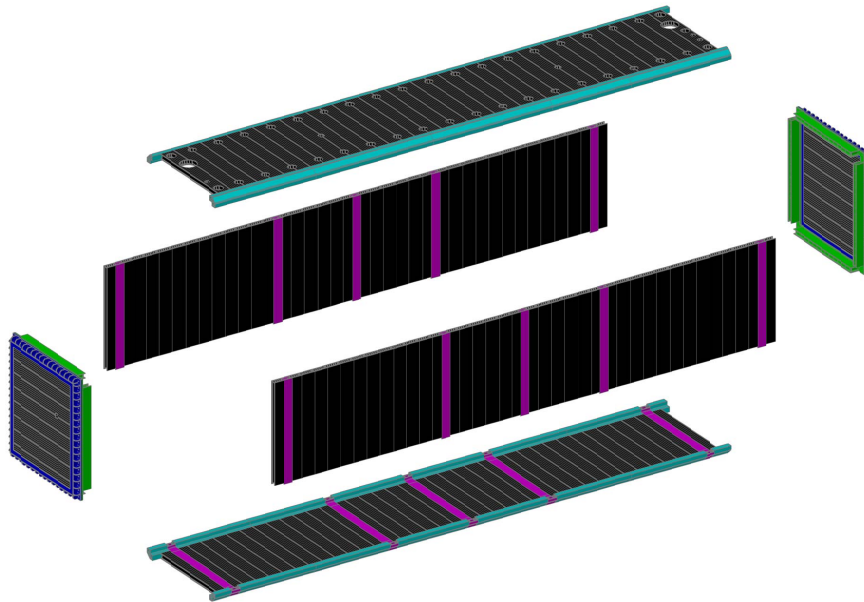


FIG. 44: *Exploded view of the whole cold vessel.*

the surface of the LAr sensitive volume. These signals would be used as anti-coincidence to identify and recognize the interactions generated by external particles.

A. CRTS efficiency

The performance of the CRTS system will depend both on the intrinsic efficiency of each CRTS detector unit and on the coverage of the adopted layout, which must approximate the ideal limit of a complete 4π solid angle.

According to the overall size of the T600 cryostat, a shell made of particle detectors with a large surface area (order of $1,000 \text{ m}^2$) will be required. The CRTS spatial granularity has to allow the unambiguous association between the reconstructed tracks in the TPC and the position where the cosmic rays cross the CRTS.

Since the TPC mixes drift time with space coordinates, a relation between the absolute time t_{true} and position y_{true} on the CRTS along the drift coordinate y is determined, as:

$$y_{true} = y_{img} + v_{drift} \cdot (t_{true} - t_0), \quad (2)$$

where y_{img} is the position on CRTS extrapolated by the recorded image on TPC, v_{drift} is the drift velocity and t_0 is the absolute trigger time opening the acquisition window. Among all the possible pairs $(t, y)_{CRTS}$ only the one satisfying Eq. 2 is considered to correctly tag the muon track crossing the CRTS. The other CRTS coordinates x and z are instead determined unambiguously.

The absolute time t_0 is expected to be obtained from the PMT system, with resolution of the order of 1 ns, in order to exploit the bunch structure of the beam. Therefore, the time resolution requested for the detectors comprising the CRTS must be at least of the same order

of magnitude. As a consequence, the uncertainty in localizing the track in space, due to the mentioned time resolution, is not less than 30 cm.

These considerations must be taken into account, when choosing the detector technology to be employed for the CRTS and its geometrical segmentation, as discussed in the next section.

B. CRTS layout

There are few well consolidated technologies to realize large-area detectors with high space and time resolution. Among these, the following may be taken into account: Resistive Plate Chambers (RPC) and plastic scintillator slabs coupled to PMTs or SiPMs. The RPCs allow building large panels (up to 3 m² of area) that can be easily arranged in large walls, but their implementation involves the use of gas mixtures and HV operation which may pose special safety issues.

A very promising detector technology, based on the use of LAr readout plates, has been proposed [29]. These plates, deployed directly inside the cryostats few centimeters away from its edges, could detect the presence of the dE/dx signals generated by the cosmic particles in the LAr with a relatively modest electric field (~ 1 kV/cm) added between the readout plates and the cryostat grounded walls. The performance of these detectors in terms of efficiency, rates, stability and noise must be carefully investigated.

The choice of the adopted detector solution must also take into account the size and shape of the T600 detector and its mechanical structure. As already discussed, the CRTS should completely surround the T600 volume, and for each side it is necessary to evaluate the most suitable technical solution, either internal or external.

The design of the top side of CRTS, which is interested by the largest amount of incoming cosmic particles flow, is certainly the most critical. Due to the presence of many dead spaces inside the TPCs, including flange feed-throughs, signal wire and HV cables, the deployment of such a detector inside the T600 will limit its effective geometrical coverage. It should be rather positioned at a suitable distance (about 3 m) from the T600 upper floor, conveniently above the readout electronics racks and the GAr recirculation units.

Similarly, vertical CRTS side walls could be more easily placed outside, positioned close to the cryostat walls, since the internal space behind the wire chambers is occupied by the PMTs, the slow control sensors and the TPC mechanical supports.

On the contrary, the bottom side CRTS detectors should be more conveniently placed into the LAr cryostat, due to the presence of the external mechanical supporting structure placed below it.

The presence of the electronics racks inside the CRTS envelope could prevent adopting a completely hermetic structure, to allow the necessary access to the TPC upper floor for maintenance and inspection purposes. For this reason, the CRTS top plane has to be kept separated from the CRTS vertical walls surrounding the T600, and the cooling system of the electronics must be carefully designed taking into account a reduced heat dissipation by natural convection.

For what concerns the future steps for a CRTS design finalization, first of all a detailed Monte Carlo simulations have to be carried out to study how to disentangle the genuine neutrino events from cosmogenic-induced backgrounds. The combined action of the CRTS and of the internal PMT system has to be studied in detail to define a possible analysis strategy for the neutrino event selection and reconstruction.

The probability of an autoveto signal by charged particles generated in the neutrino inter-

actions and escaping the LAr-TPCs has to be carefully evaluated. According to results of a preliminary evaluation, considering the CTRS system installed inside the cryostats and surrounding the LAr volume, $\sim 45\%$ of ν_μ CC and $\sim 10\%$ of ν_e events are expected to provide a signal. Alternatively $\sim 10\%$ of ν_μ and few percent of ν_e events are expected to give a signal in an external muon tagging system.

The T600 CRTS must be realized in a common framework with the LAr1-ND CRTS, being mandatory for the two detectors to adopt the same design of the cosmic ray detection efficiency with identical sensitivities and systematics.

-
- [1] F.J. Hasert *et al.*, “Search for elastic muon-neutrino electron scattering,” *Physics Letters B* **46**, 121 – 124 (1973).
 - [2] F.J. Hasert *et al.*, “Observation of neutrino-like interactions without muon or electron in the Gargamelle neutrino experiment,” *Physics Letters B* **46**, 138 – 140 (1973).
 - [3] C. Rubbia, “The Liquid Argon Time Projection Chamber: A New Concept for Neutrino Detectors,” (1977).
 - [4] P. Benetti *et al.*, “A three-ton liquid argon time projection chamber,” *Nucl.Instrum.Meth.* **A332**, 395 – 412 (1993).
 - [5] P. Cennini *et al.*, “Performance of a three-ton liquid argon time projection chamber,” *Nucl.Instrum.Meth.* **A345**, 230 – 243 (1994).
 - [6] F. Arneodo *et al.*, “First observation of 140-cm drift ionizing tracks in the ICARUS liquid-argon TPC,” *Nucl.Instrum.Meth.* **A449**, 36 – 41 (2000).
 - [7] P Cennini *et al.*, “Detection of scintillation light in coincidence with ionizing tracks in a liquid argon time projection chamber,” *Nucl.Instrum.Meth.* **A432**, 240 – 248 (1999).
 - [8] F Arneodo *et al.*, “Performance of the 10m3 ICARUS liquid argon prototype,” *Nucl.Instrum.Meth.* **A498**, 292 – 311 (2003).
 - [9] S. Amerio *et al.* (ICARUS Collaboration), “Design, construction and tests of the ICARUS T600 detector,” *Nucl.Instrum.Meth.* **A527**, 329–410 (2004).
 - [10] C. Rubbia, M. Antonello, P. Aprili, B. Baibussinov, M. Baldo Ceolin, *et al.*, “Underground operation of the ICARUS T600 LAr-TPC: first results,” *JINST* **6**, P07011 (2011), [arXiv:1106.0975 \[hep-ex\]](https://arxiv.org/abs/1106.0975).
 - [11] M Antonello, B Baibussinov, P Benetti, E Calligarich, N Canci, *et al.*, “Experimental search for the LSND anomaly with the ICARUS detector in the CNGS neutrino beam,” *Eur.Phys.J.* **C73**, 2345 (2013), [arXiv:1209.0122 \[hep-ex\]](https://arxiv.org/abs/1209.0122).
 - [12] M Antonello, B Baibussinov, P Benetti, E Calligarich, N Canci, *et al.*, “Search for anomalies in the ν_e appearance from a ν_μ beam,” *Eur.Phys.J.* **C73**, 2599 (2013), [arXiv:1307.4699 \[hep-ex\]](https://arxiv.org/abs/1307.4699).
 - [13] M. Antonello *et al.*, “Measurement of the neutrino velocity with the ICARUS detector at the CNGS beam,” *Physics Letters B* **713**, 17 – 22 (2012).
 - [14] M. Antonello *et al.*, “Precision measurement of the neutrino velocity with the icarus detector in the cngs beam,” *Journal of High Energy Physics* **2012**, 49 (2012), [10.1007/JHEP11\(2012\)049](https://arxiv.org/abs/10.1007/JHEP11(2012)049).
 - [15] M. Antonello, B. Baibussinov, P. Benetti, F. Boffelli, A. Bubak, *et al.*, “Experimental observation of an extremely high electron lifetime with the ICARUS-T600 LAr-TPC,” (2014), [10.1088/1748-0221/9/12/P12006](https://arxiv.org/abs/10.1088/1748-0221/9/12/P12006), [arXiv:1409.5592 \[physics.ins-det\]](https://arxiv.org/abs/1409.5592).
 - [16] B. Baibussinov *et al.*, “A new, very massive modular Liquid Argon Imaging Chamber to detect low energy off-axis neutrinos from the CNGS beam (Project MODULAR),” *Astroparticle Physics*

- [29](#), 174 – 187 (2008).
- [17] D Angeli *et al.*, “Towards a new Liquid Argon Imaging Chamber for the MODULAR project,” *Journal of Instrumentation* **4**, P02003 (2009).
- [18] G. Mention, M. Fechner, Th. Lasserre, Th.A. Mueller, D. Lhuillier, *et al.*, “The Reactor Antineutrino Anomaly,” *Phys.Rev.* **D83**, 073006 (2011), [arXiv:1101.2755 \[hep-ex\]](#).
- [19] W. Hampel *et al.* (GALLEX Collaboration), “Final results of the Cr-51 neutrino source experiments in GALLEX,” *Phys.Lett.* **B420**, 114–126 (1998).
- [20] J.N. Abdurashitov *et al.* (SAGE Collaboration), “Measurement of the response of the Russian-American gallium experiment to neutrinos from a Cr-51 source,” *Phys.Rev.* **C59**, 2246–2263 (1999), [arXiv:hep-ph/9803418 \[hep-ph\]](#).
- [21] A. Aguilar-Arevalo *et al.* (LSND Collaboration), “Evidence for neutrino oscillations from the observation of anti-neutrino(electron) appearance in a anti-neutrino(muon) beam,” *Phys.Rev.* **D64**, 112007 (2001), [arXiv:hep-ex/0104049 \[hep-ex\]](#).
- [22] A.A. Aguilar-Arevalo *et al.* (MiniBooNE Collaboration), “A Search for electron neutrino appearance at the $\Delta m^2 \sim 1 \text{ eV}^2$ scale,” *Phys.Rev.Lett.* **98**, 231801 (2007), [arXiv:0704.1500 \[hep-ex\]](#).
- [23] A.A. Aguilar-Arevalo *et al.* (MiniBooNE Collaboration), “Unexplained Excess of Electron-Like Events From a 1-GeV Neutrino Beam,” *Phys.Rev.Lett.* **102**, 101802 (2009), [arXiv:0812.2243 \[hep-ex\]](#).
- [24] A.A. Aguilar-Arevalo *et al.* (MiniBooNE Collaboration), “Improved Search for $\bar{\nu}_\mu \rightarrow \bar{\nu}_e$ Oscillations in the MiniBooNE Experiment,” *Phys.Rev.Lett.* **110**, 161801 (2013), [arXiv:1207.4809 \[hep-ex\]](#).
- [25] Giuseppe Battistoni, S. Muraro, Paola R. Sala, Fabio Cerutti, A. Ferrari, *et al.*, “The FLUKA code: Description and benchmarking,” *AIP Conf.Proc.* **896**, 31–49 (2007).
- [26] A. Ferrari, P.R. Sala, A. Fassò, and J. Ranft, *FLUKA: a multi-particle transport code*, Tech. Rep. CERN-2005-10, INFN/TC_05/11, SLAC-R-773 (CERN, 2005).
- [27] G. Battistoni, A. Ferrari, M. Lantz, P. R. Sala, and G. I. Smirnov, “A neutrino-nucleon interaction generator for the FLUKA Monte Carlo code,” in *CERN-Proceedings-2010-001*, pp. 387–394.
- [28] <http://www.numi.fnal.gov>.
- [29] C. Rubbia, “Searching for short baseline anomalies with the LAr-TPC detector at shallow depths,” (2014), [arXiv:1408.6431 \[physics.ins-det\]](#).
- [30] for the ICARUS Collaboration C. Rubbia, “Using the beam bunch-structure with the T600 detector,” internal SBN report (2014).
- [31] S. Amoruso *et al.*, “Study of electron recombination in liquid argon with the ICARUS TPC,” *Nucl.Instrum.Meth.* **A523**, 275 – 286 (2004).
- [32] A. Ankowski *et al.*, “Characterization of ETL 9357FLA photomultiplier tubes for cryogenic temperature applications,” *Nucl.Instrum.Meth.* **A556**, 146 – 157 (2006).
- [33] P. Benetti, C. Montanari, G.L. Raselli, M. Rossella, and C. Vignoli, “Detection of the VUV liquid argon scintillation light by means of glass-window photomultiplier tubes,” *Nucl.Instrum.Meth.* **A505**, 89 – 92 (2003), proceedings of the tenth Symposium on Radiation Measurements and Applications.
- [34] M Antonello *et al.*, “The trigger system of the ICARUS experiment for the CNGS beam,” *Journal of Instrumentation* **9**, P08003 (2014).
- [35] <http://www.airliquide.it/>.
- [36] <http://www.stirlingcryogenics.com/>.
- [37] A. Falcone *et al.*, “Comparison between large area photo-multiplier tubes at cryogenic temperature for neutrino and rare event physics experiments,” *Nucl.Instrum.Meth.* , – (2014).

-
- [38] B. Baibussinov *et al.*, “The ICARUS Front-end Preamplifier Working at Liquid Argon Temperature,” ArXiv e-prints (2011), [arXiv:1108.3825](https://arxiv.org/abs/1108.3825) [physics.ins-det].
- [39] M. Lipinski *et al.*, “Performance results of the first white rabbit installation for cngs time transfer,” in *Precision Clock Synchronization for Measurement Control and Communication (ISPCS), 2012 International IEEE Symposium on* (2012) pp. 1–6.
- [40] <http://www.gtt.fr>.
- [41] <http://www.ihl.co.jp/en>.